1996PASP..108..277O

Publications of the Astronomical Society of the Pacific
108: 277–308, 1996 March

Night-Sky High-Resolution Spectral Atlas of OH and O_2 Emission Lines for Echelle Spectrograph Wavelength Calibration[1,2]

DONALD E. OSTERBROCK, JON P. FULBRIGHT, ANDRÉ R. MARTEL, MICHAEL J. KEANE, AND SCOTT C. TRAGER

University of California Observatories/Lick Observatory, Board of Studies in Astronomy and Astrophysics, University of California, Santa Cruz, California 95064
Electronic mail: don@ucolick.org, jfulb@ucolick.org, amartel@ucolick.org, mk@ucolick.org, sctrager@ucolick.org

GIBOR BASRI

Department of Astronomy, University of California, Berkeley, California 94720
Electronic mail: basri@soleil.berkeley.edu

Received 1995 September 26; accepted 1995 December 5

ABSTRACT. The potential of night-sky emission lines recorded on every long-exposure astronomical spectrum, for wavelength calibration, is emphasized. A high-resolution atlas, based on spectra obtained with the Keck 10-m telescope on Mauna Kea and the high-resolution echelle spectrograph (HIRES) is presented. This atlas shows OH, O_2, and a few other night-sky lines, and will make it possible to identify them easily on high-resolution spectra. Accurate wavelengths and references to their sources are given.

1. INTRODUCTION

The emission lines of the night-sky spectrum are a nuisance in astronomy; they are recorded in every observed spectrum of a star, nebula, or galaxy, and if the object is faint and the exposure time correspondingly long, the night-sky lines seriously contaminate its spectrum. Particularly in the red and infrared there are many lines of the Meinel (1950a) OH (vibration–rotation) bands. We remove them as well as we can by subtracting sky spectra, and the limiting accuracy in measuring line or continuum intensities is often determined by these night-sky lines.

However, there is also a positive aspect to the night-sky lines. Since they are registered on every spectrum, they represent a potential wavelength calibration or zero-point determination which is taken automatically for the same exposure time, with the telescope and spectrograph in the same orientation, etc. For the low-dispersion spectra of galaxies taken at Lick Observatory, many observers use the sky lines to fix the wavelength zero point of each exposure. They thus provide the possibility of measuring accurate radial velocities or redshifts without taking time-consuming comparison spectra before and/or after each galaxy spectrum, without moving the telescope. Osterbrock and Martel (1992) published an atlas and list of accurate wavelengths, in particular for the numerous OH lines. Many observers have found this paper useful for finding, identifying and using the sky lines on their spectra.

With the Keck 10-m telescope, the high-resolution echelle spectrograph (HIRES) has proven to be a fast, reliable instrument (Vogt et al. 1994). Several observers have used it to observe galaxies. Since each order of the echelle spectrum includes only a limited range of wavelength, numerous sky lines should be useful for providing a wavelength zero point or check in each order. The low-dispersion atlas is not at all well suited for use with these HIRES spectra. Hence we have prepared a new, high-resolution atlas to be used with it, or with similar high-dispersion echelle spectrographs at other observatories.

2. OBSERVATIONAL DATA

The atlas was assembled from three pairs of exposures plus one single exposure taken with HIRES by various observers in the course of their regular programs, as listed in Table 1. The currently available CCDs are not large enough to cover the entire length of the orders in a single exposure, but by using two settings of the echelle, "left" and "right," it is possible to do so, with an overlap in the middle. The night-sky spectrum was extracted from each exposure ("above" and "below" the object spectrum), and these three pairs of exposures were combined to get the maximum spectral coverage. The single exposure was used to fill in the last remaining gap. The resulting night-sky spectrum extends from λ3856 (in order 92) to λ8995 (in order 40). The slit widths were chosen to give a resolution ~0.2 Å at λ7000 in each case, while the dispersion at the CCD was 0.05 Å/pixel. Hence the spectra were well sampled. One of the spectra had been binned in order to increase the signal-to-noise ratio, so for it the dispersion was ~0.1 Å/pixel. In the atlas it was only used for order 55 and part of 54.

The wavelength scale was calibrated on each exposure by the OH lines themselves. Once the dispersion solution had been applied to all the orders, the whole echelle spectrum was extracted into its individual orders, which are plotted in

[1]Lick Observatory Bulletin 1327.
[2]Based on observations obtained at the W. M. Keck Observatory, which is operated by the California Institute of Technology and the University of California.

© 1996. Astronomical Society of the Pacific

© Astronomical Society of the Pacific • Provided by the NASA Astrophysics Data System

1996PASP..108..277O

TABLE 1
Journal of Night-Sky-Spectra Observations

Observers	Vogt/Keane		Vogt/Churchill	Basri		Sargent/Barlow	
	left	right		left	right	left	right
Date	1994 Oct 9		1995 Jan 24	23 Nov 1994	1995 Mar 12	23 Feb 1995	
UT	12:10	14:28	14:51	7:18	6:23	9:27	12:12
Orders	92–57		82–53	55–41		54–40	
λλ	3865–6305		4320–6760	6388–8730		6510–8995	
Exp.	90 min.		30 min.	60 min.		50 min.	
α (1950)	$2^h07'$		$12^h13'$	$1^h25'$	$3^h45'$	$12^h03'$	
δ (1950)	$-0°19'$		$-0°17'$	$+27°50'$	$+23°30'$	$-7°26'$	
Zen. Dist. (°)	26	44	22	80	49	50	28
Azimuth (°)	184	238	199	32	76	120	178

Figs. 1 through 26. The continuum was flattened by fitting a spline to each order, and the intensity scale for each order was normalized so that its strongest line would peak at 1.00. This means that each order was normalized by a different factor, but the peaks of lines in common to two successive orders, and/or the noise level can be used to estimate the relative strengths of features on different orders Note that on two orders (61 and 64) the strengths of the atomic lines (Na I λ5890 and [O I] λ5577, respectively) are so great that the OH lines would not be visible on the plots with this scaling. The scale on the abscissae for these two orders can be used to determine the relative strengths of the OH lines to the atomic lines on these two orders.

Night-sky lines are visible in the spectra only longwards of λ5200. Hence no orders at shorter wavelengths than this (orders larger than 68) were plotted in the figures. Also, no night-sky features were seen in order 62, nor in orders 65–67, and they were not plotted either. Two of the spectra used have considerable overlap in the range λλ6500–8700. Although they were taken at different times on different dates at different positions in the sky, there are no striking differences in relative intensities among the spectra, except for the [O I] lines mentioned in Sect. 5. This atlas should provide a good starting point for identifying night-sky lines for wavelength calibration purposes anywhere in the sky.

3. OH BANDS

Most of the night-sky lines are from the Meinel rotation–vibration bands of OH. Since our low-dispersion atlas (Osterbrock and Martel 1992) appeared, much better wavelengths for these lines, accurate to 0.00001 Å, have been measured in the laboratory, calculated, and published by Abrams et al. (1994). Hence in the figures we label the OH lines by their designations in the standard spectroscopic notation used by these authors, and give the wavelength to 0.001 Å from their list. These wavelengths, listed in their Table 29, should be used. They are tabulated in the standard spectroscopic notation described by Herzberg (1950). The ground electronic term of OH has the projection of the electronic angular momentum on the nuclear axis $\Lambda=1$, and projection of the spin angular momentum $\Sigma=\frac{1}{2}$. Hence it is a $^2\Pi$ term, and its coupling is close to Hund's case (a). It is inverted; the ground electronic level is $^2\Pi_{\frac{3}{2}}$ with total electronic angular momentum about the internuclear axis $\Omega=\frac{3}{2}$, while the first excited electronic level is $^2\Pi_{\frac{1}{2}}$ with $\Omega=\frac{1}{2}$. The total rotational angular momentum J is then the vector sum of Ω and N, the angular momentum of molecular rotation, so $J=\Omega,\Omega+1,\Omega+2,\ldots$. The vibrational quantum number is $v=0,1,2,\ldots$. A vibration–rotation transition occurs between an upper level v',J' and a lower level v'',J'' of the same electronic term. Those within the ground $^2\Pi_{\frac{3}{2}}$ are labeled $(v'-v'')R_1(J'')$, $Q_1(J'')$, or $P_1(J'')$ according as $J'-J''=1$, 0, or -1. The transitions within the first excited $^2\Pi_{\frac{1}{2}}$ are correspondingly labeled $(v'-v'')_2(J'')$, $Q_2(J'')$, or $P_2(J'')$. Because of the higher excitation energies of their upper levels and the temperature of the OH-emitting layer of the atmosphere, the $^2\Pi_{\frac{1}{2}}$ tend to be roughly one-third as strong as the corresponding $^2\Pi_{\frac{3}{2}}$ lines. Each rotational line is further split by Λ-type doubling into two components, labeled with subscripts e and f in the current notation, depending on the parity of the electronic wave functions to reflection in a plane through the internuclear axis. The selection rule is that the R and P lines connect e levels only with e, and f only with f, while Q lines connect only e with f. The two separate components of each line are labeled with the e or f of the upper level, for example $P_{1e}(3.5)$ and $P_{1f}(3.5)$.

This standard spectroscopic notation differs from that used in the earlier astronomical literature, beginning with Meinel (1950) and Chamberlain (1961), and continued for convenience of comparison with them by Osterbrock and Martel (1992). The relation between the two notations is described in the latter paper. The OH lines, the most numerous by far in the night-sky spectrum in the optical and infrared regions, are identified in our Figs. 1 through 26 as above, except that in accordance with Abrams et al. (1994) the subscripts are printed on the line, to save space.

The Λ-type splitting increases with increasing J, and for most bands the lines of smaller J are unresolved even at the echelle resolution. Both from theory and from observation of the lines split widely enough to be resolvable, the two components of each line are expected to have essentially equal intensities. Thus for the lines which are not resolved, the straight arithmetic mean of the wavelengths of the two lines is given on the plots, and the blended line is labeled without the symmetry property e or f. Since for HIRES, with the slit width commonly used the resolution is ~0.2 Å, we adopted this specific separation as the boundary between two compo-

© Astronomical Society of the Pacific • Provided by the NASA Astrophysics Data System

1996PASP..108..277O

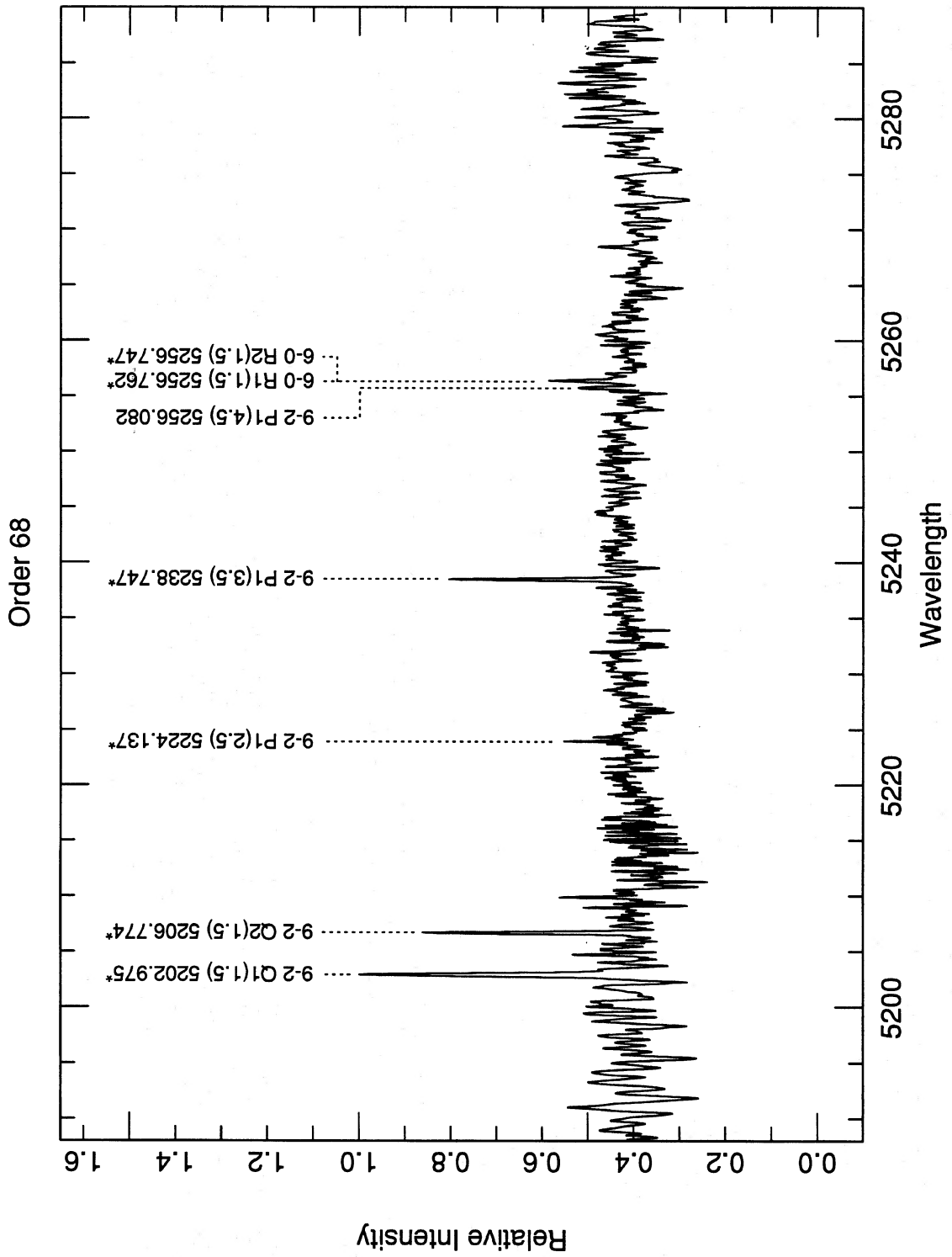

FIG. 1—Order 68 of Mauna Kea night-sky emission-line spectrum.

© Astronomical Society of the Pacific • Provided by the NASA Astrophysics Data System

1996PASP..108..277O

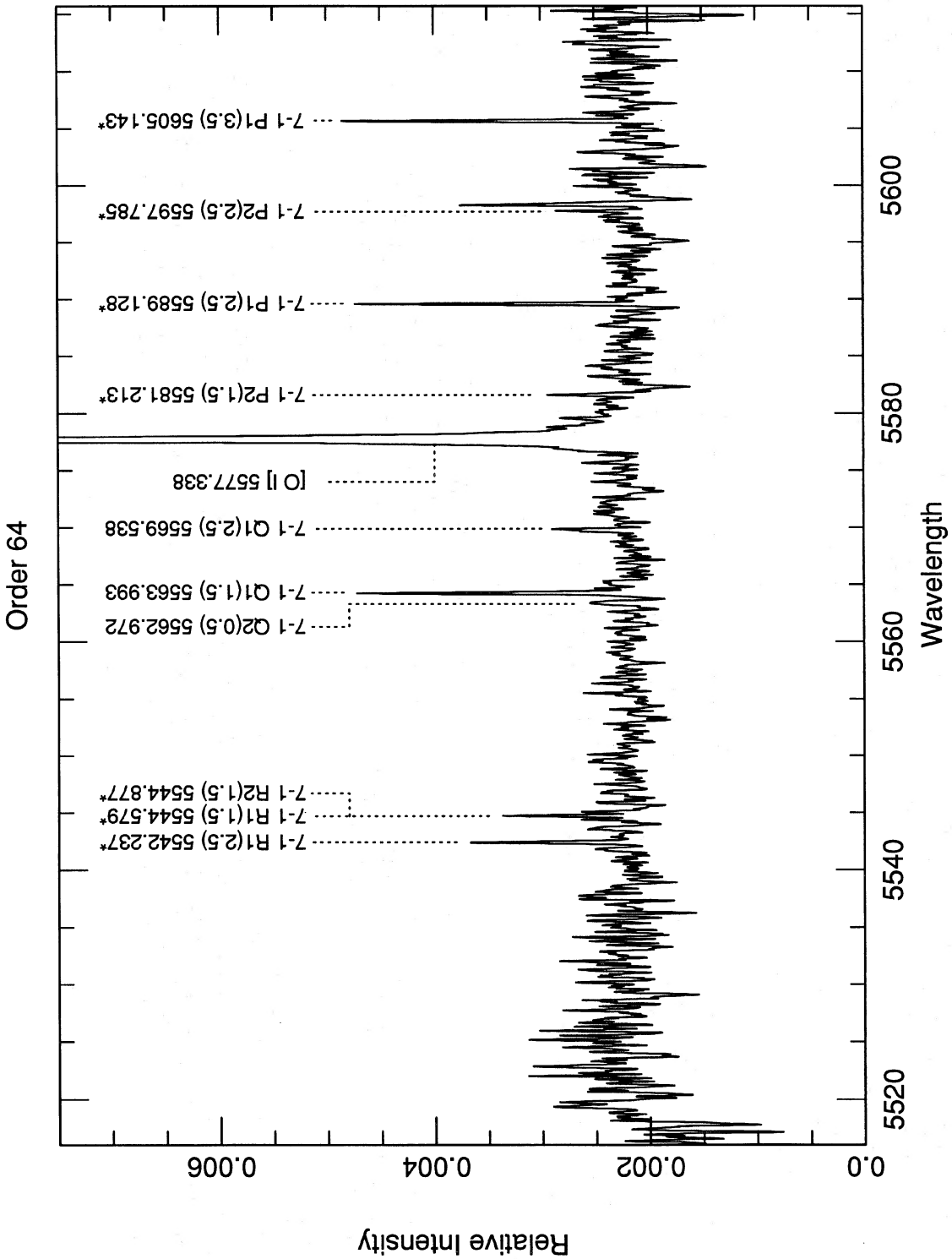

FIG. 2—Order 64 of Mauna Kea night-sky emission-line spectrum.

© Astronomical Society of the Pacific • Provided by the NASA Astrophysics Data System

1996PASP..108..277O

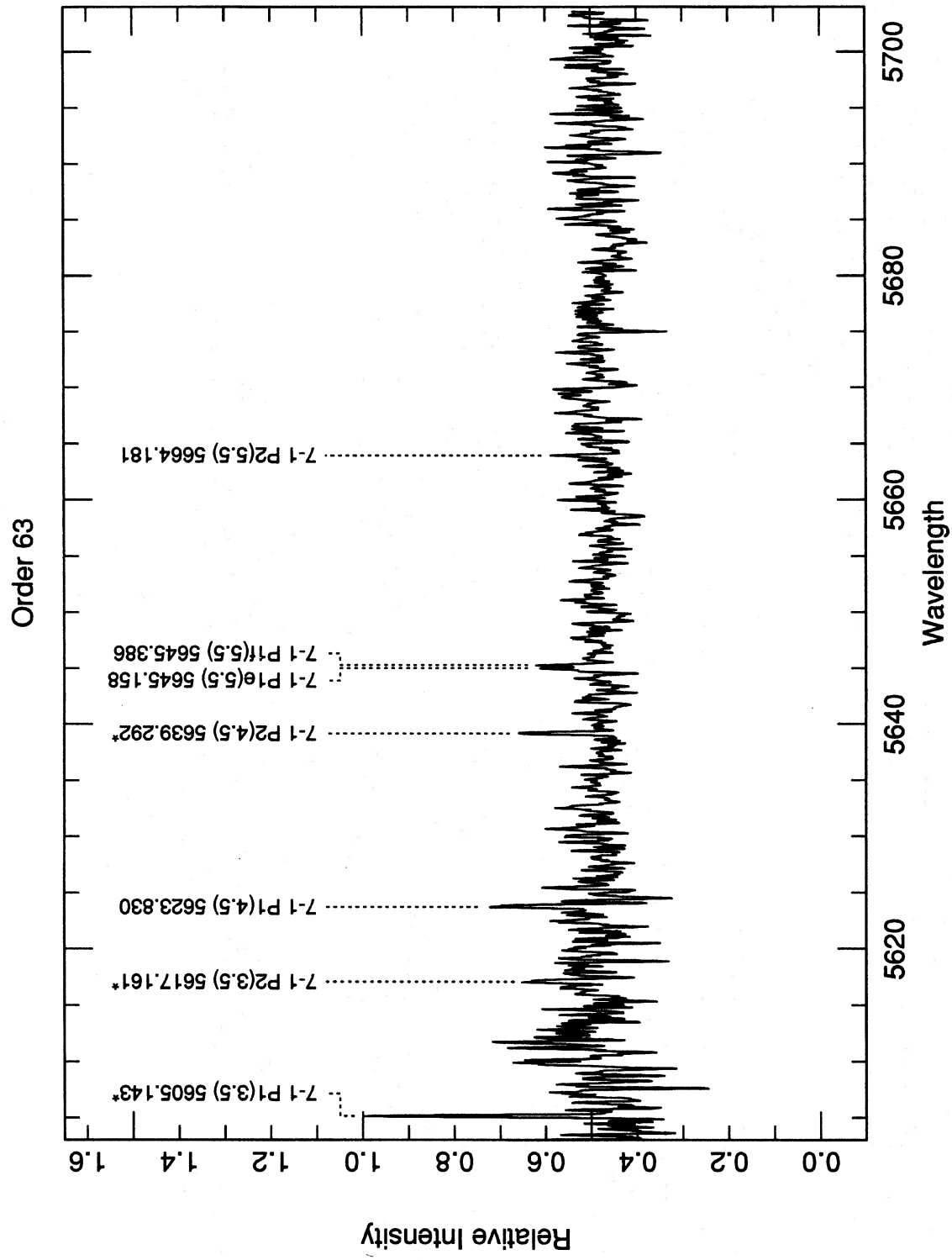

FIG. 3—Order 63 of Mauna Kea night-sky emission-line spectrum.

© Astronomical Society of the Pacific • Provided by the NASA Astrophysics Data System

1996PASP..108..277O

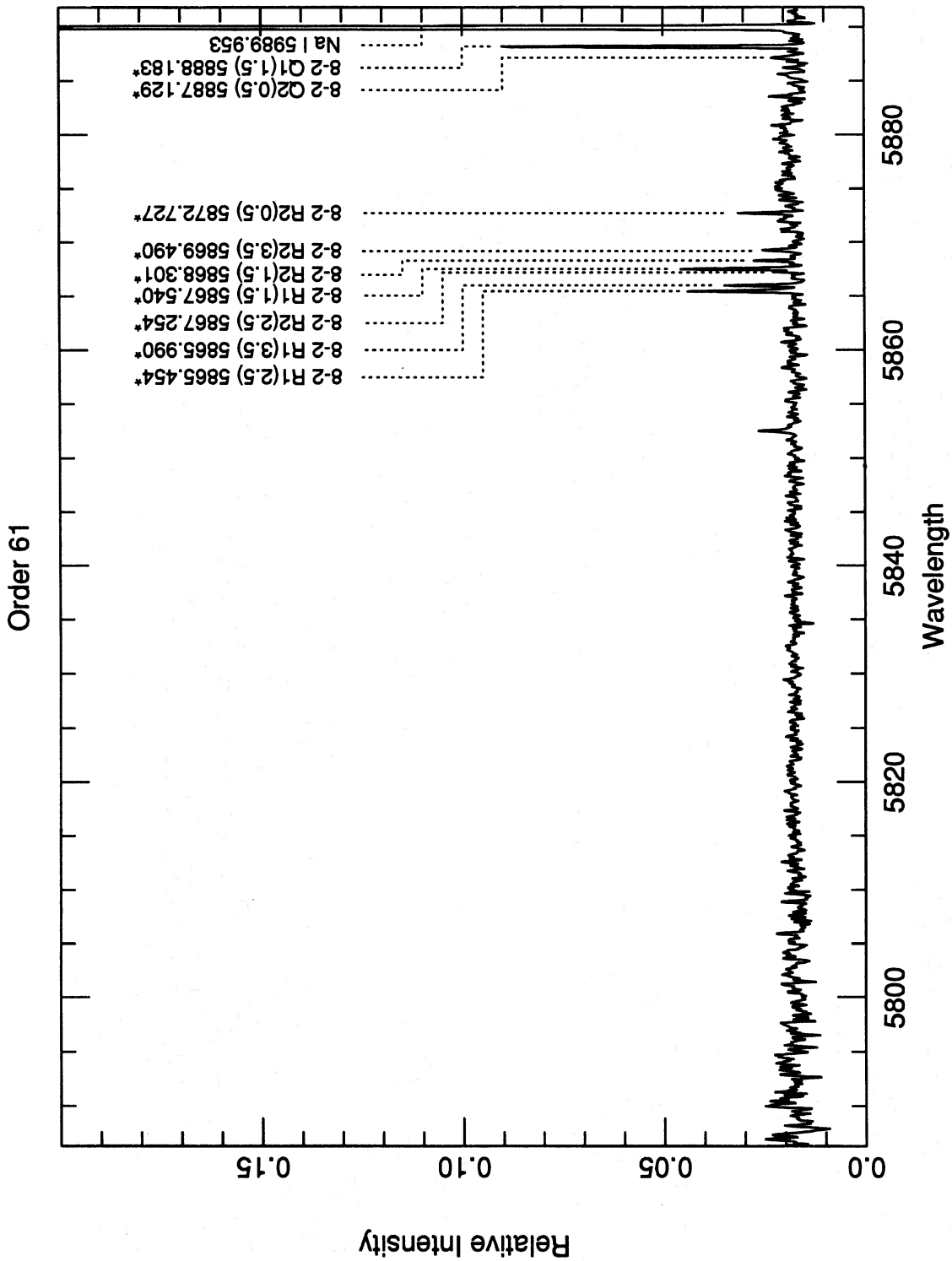

FIG. 4—Order 61 of Mauna Kea night-sky emission-line spectrum.

© Astronomical Society of the Pacific • Provided by the NASA Astrophysics Data System

1996PASP..108..277O

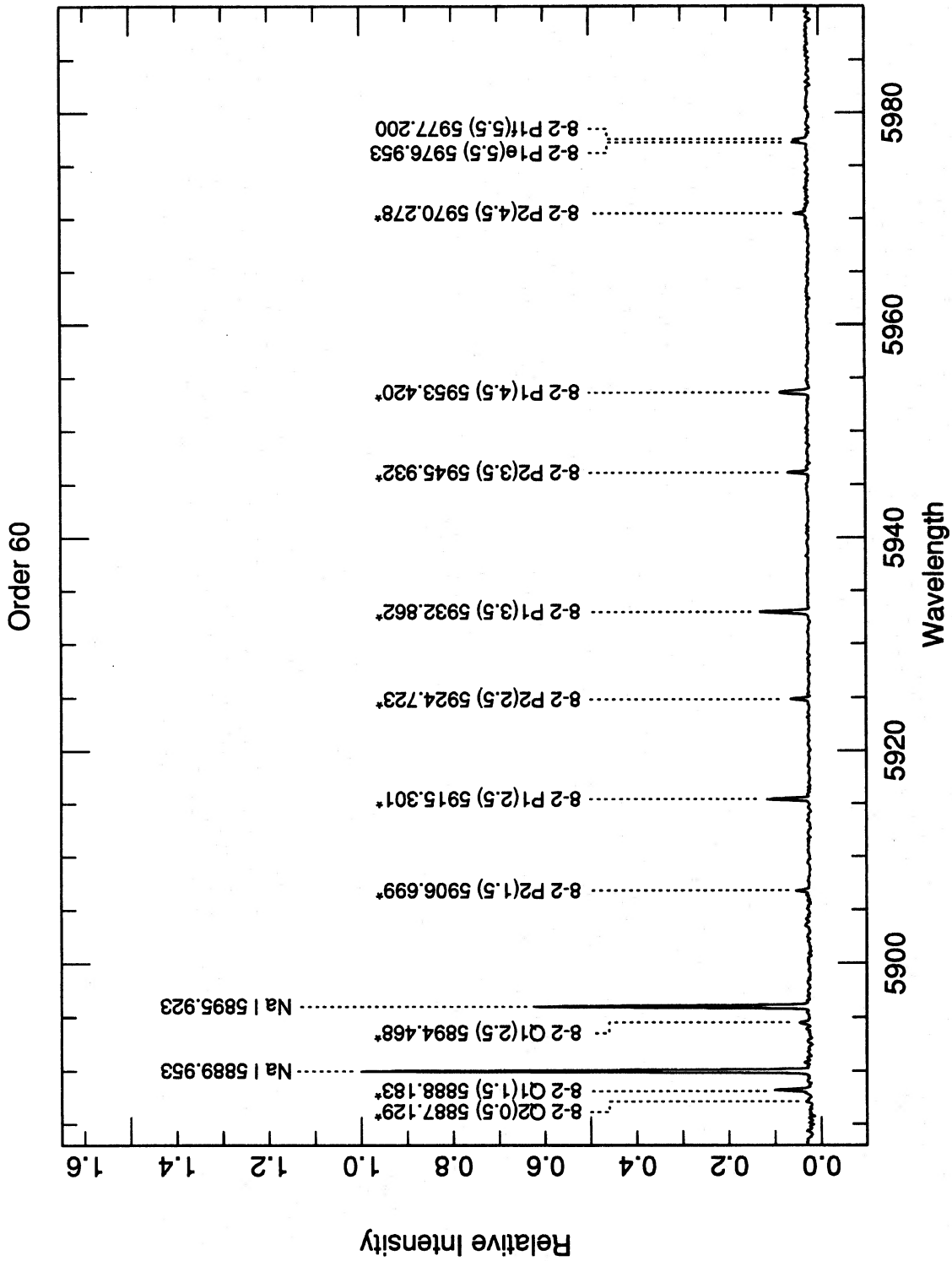

FIG. 5—Order 60 of Mauna Kea night-sky emission-line spectrum.

© Astronomical Society of the Pacific • Provided by the NASA Astrophysics Data System

1996PASP..108..277O

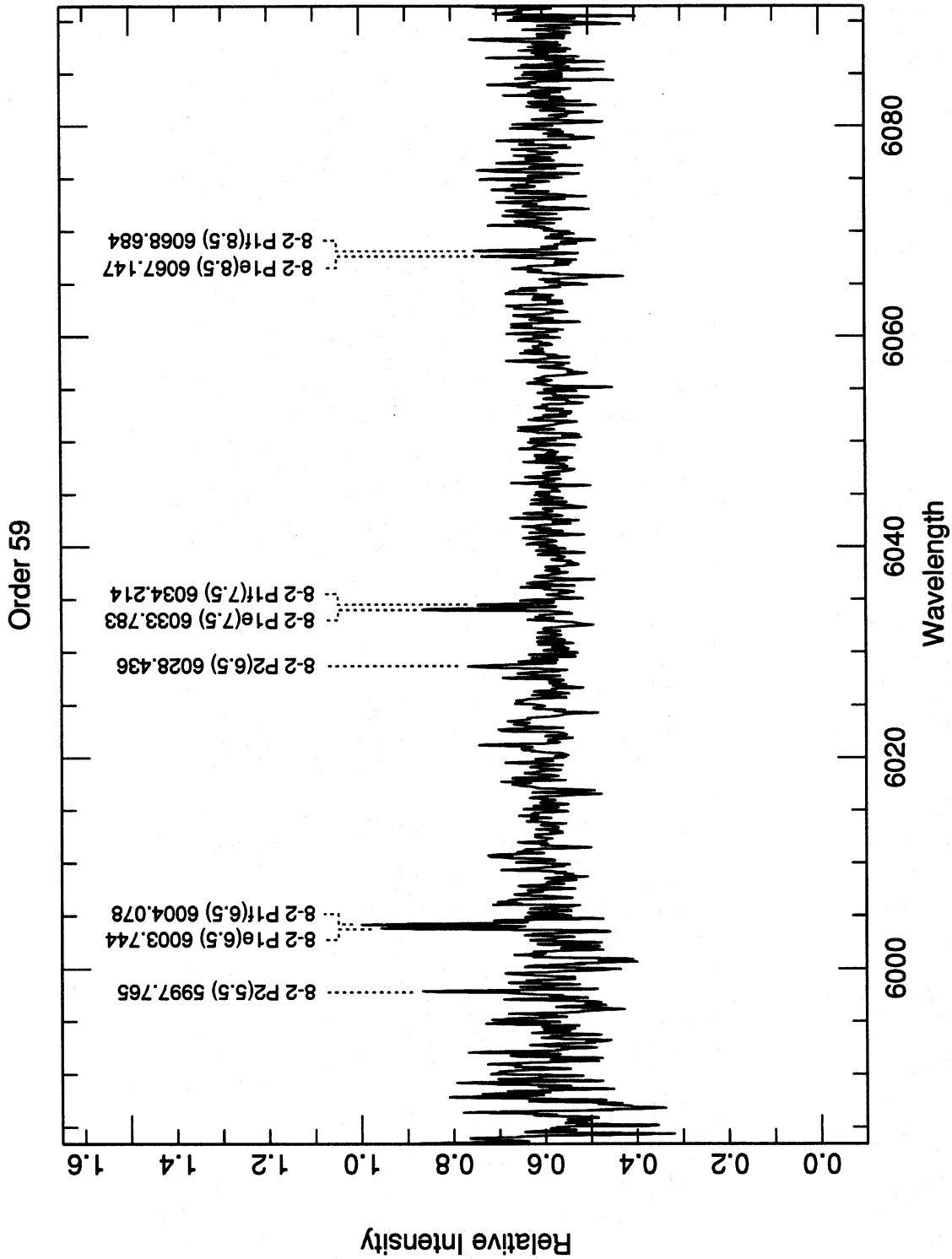

FIG. 6—Order 59 of Mauna Kea night-sky emission-line spectrum.

© Astronomical Society of the Pacific • Provided by the NASA Astrophysics Data System

1996PASP..108..277O

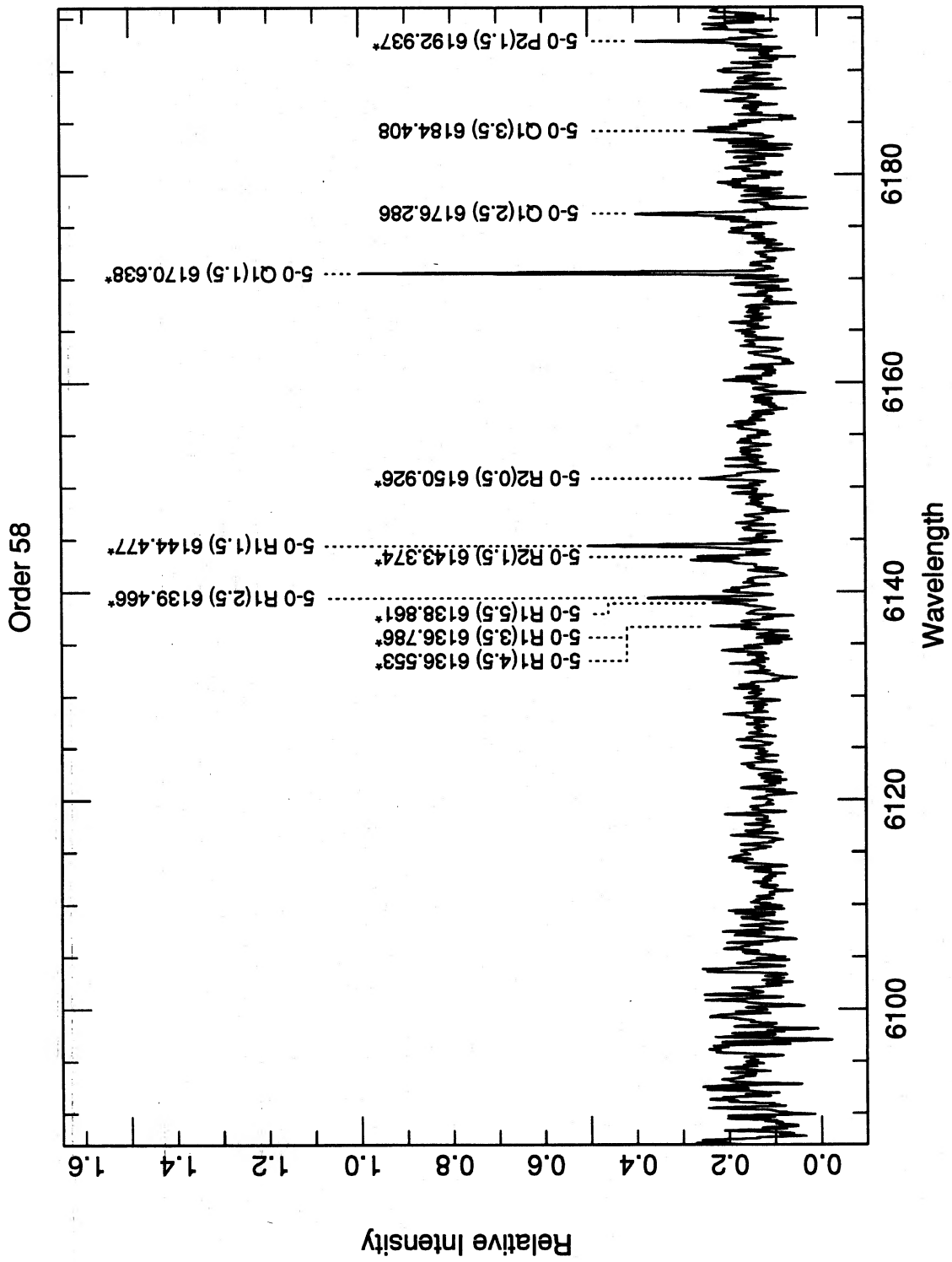

FIG. 7—Order 58 of Mauna Kea night-sky emission-line spectrum.

© Astronomical Society of the Pacific • Provided by the NASA Astrophysics Data System

1996PASP..108..277O

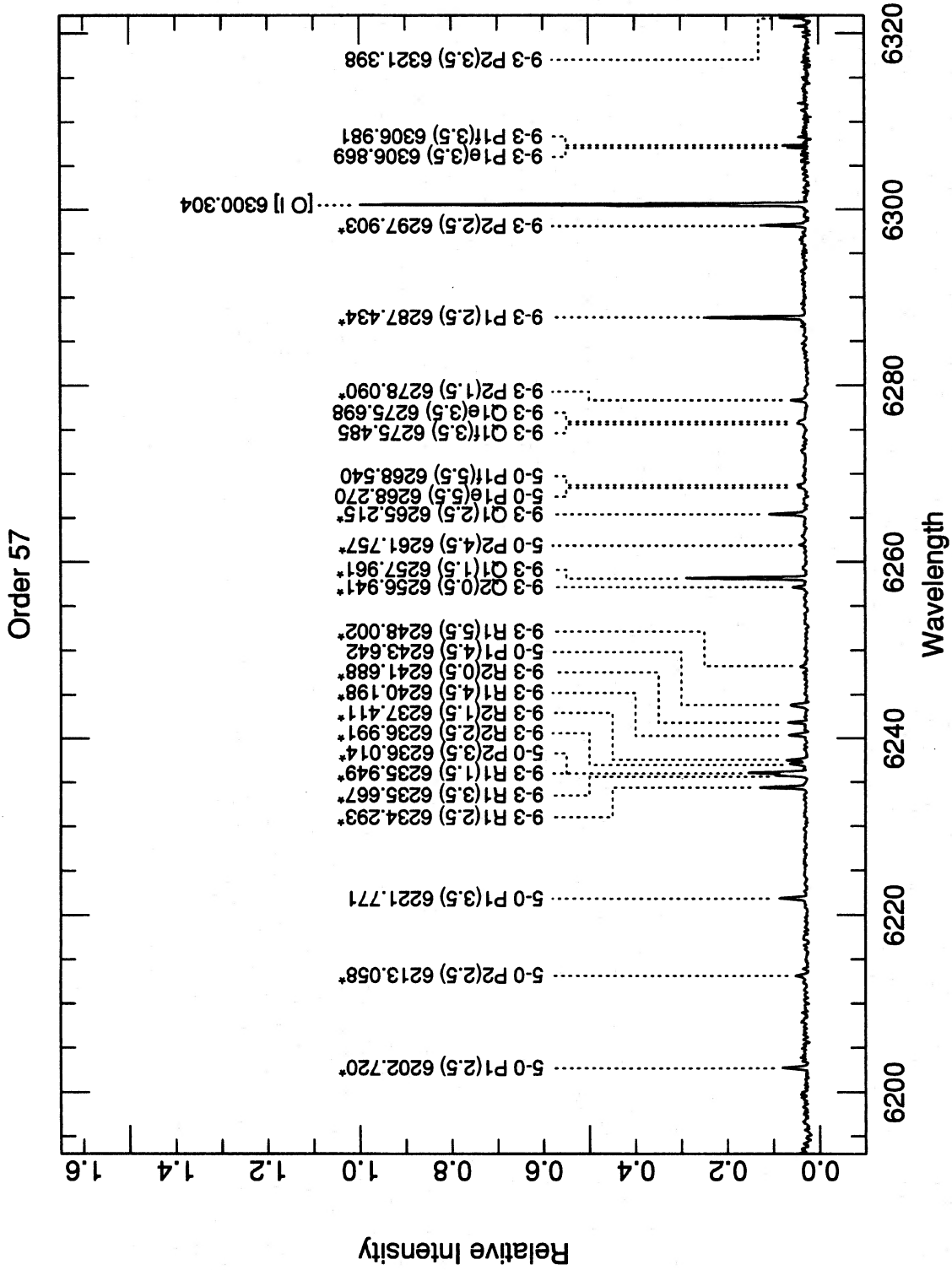

FIG. 8—Order 57 of Mauna Kea night-sky emission-line spectrum.

© Astronomical Society of the Pacific • Provided by the NASA Astrophysics Data System

1996PASP..108..277O

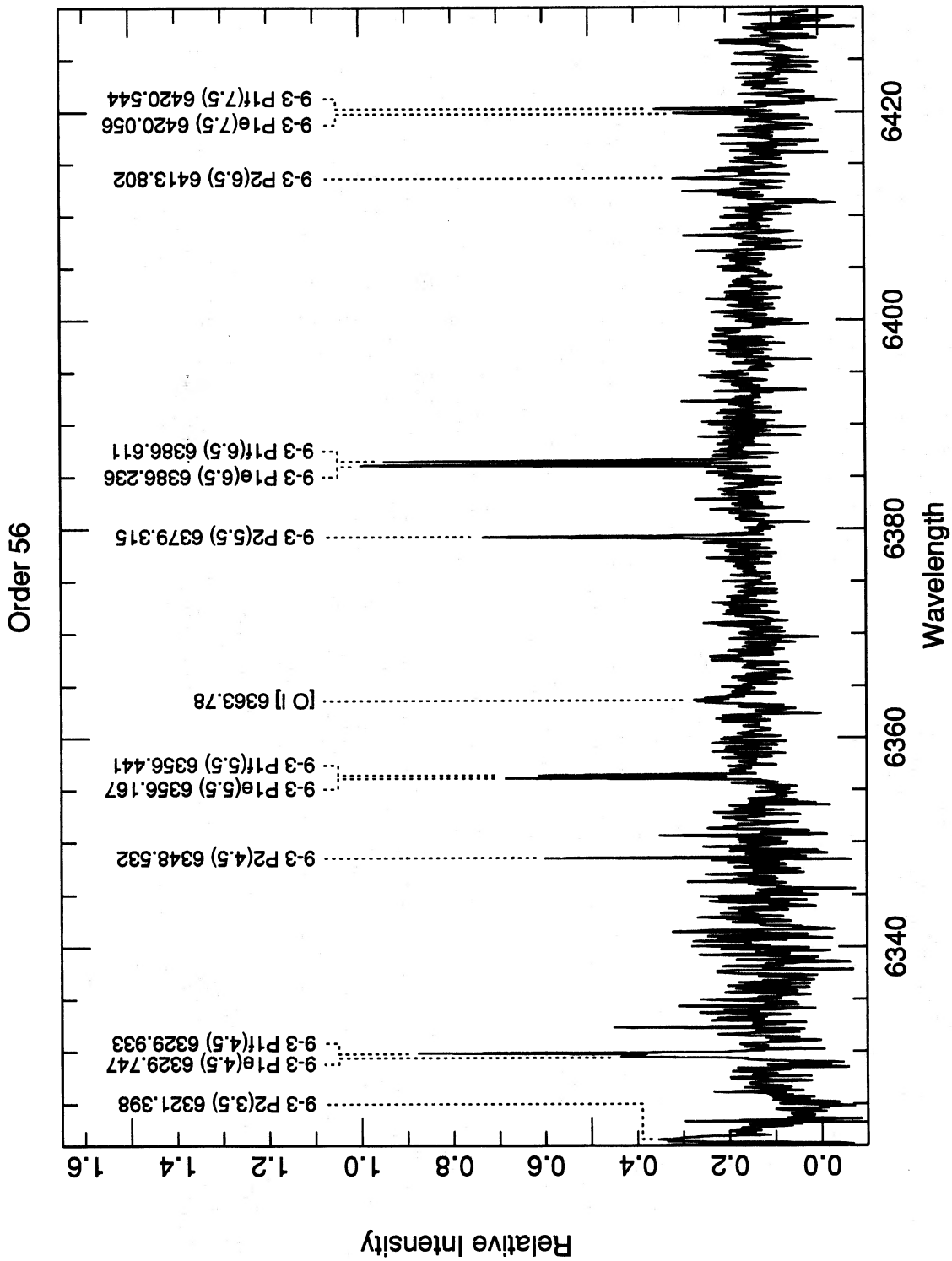

FIG. 9—Order 56 of Mauna Kea night-sky emission-line spectrum.

© Astronomical Society of the Pacific • Provided by the NASA Astrophysics Data System

1996PASP..108..2770

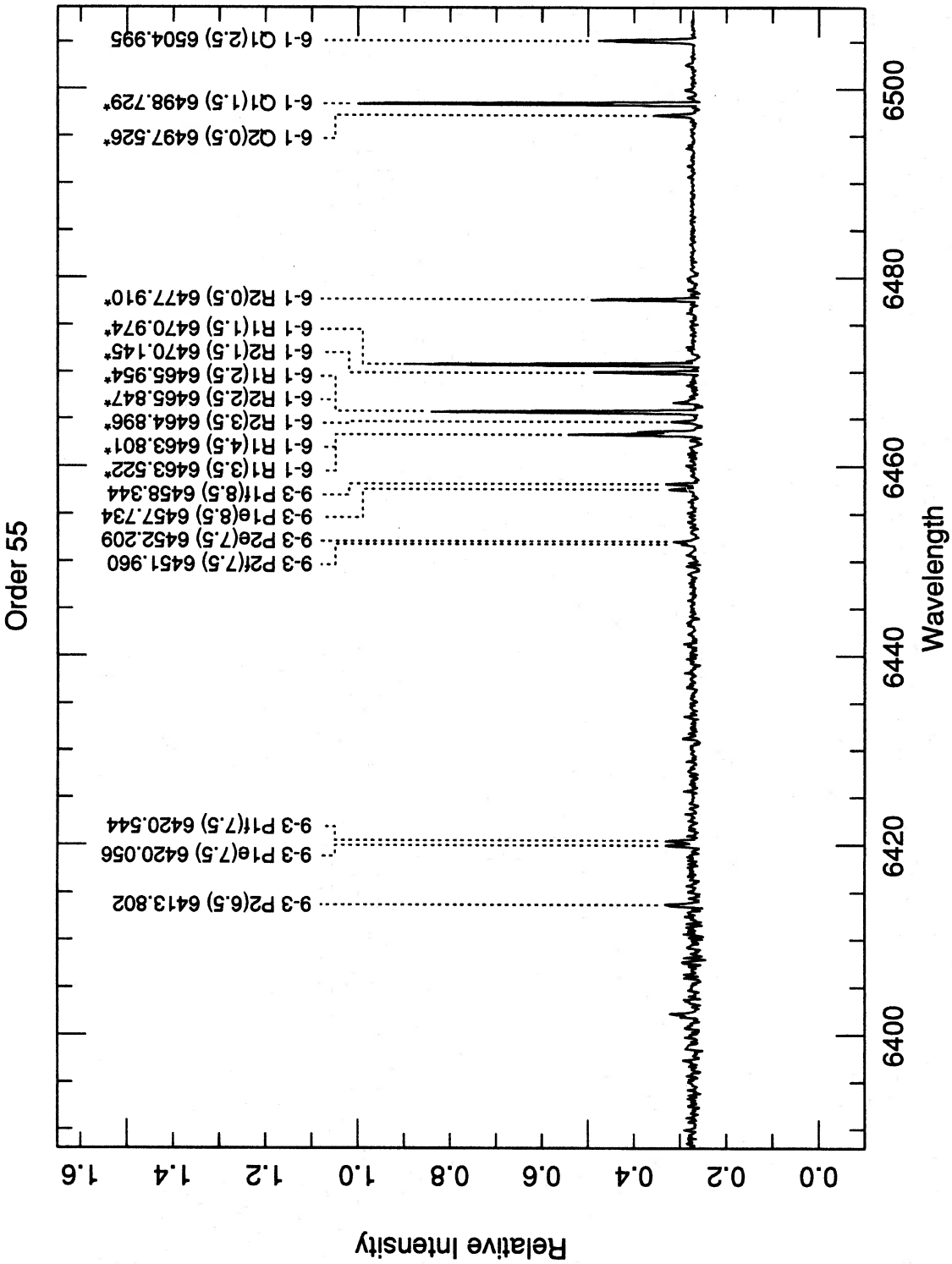

FIG. 10—Order 55 of Mauna Kea night-sky emission-line spectrum.

© Astronomical Society of the Pacific • Provided by the NASA Astrophysics Data System

1996PASP..108..277O

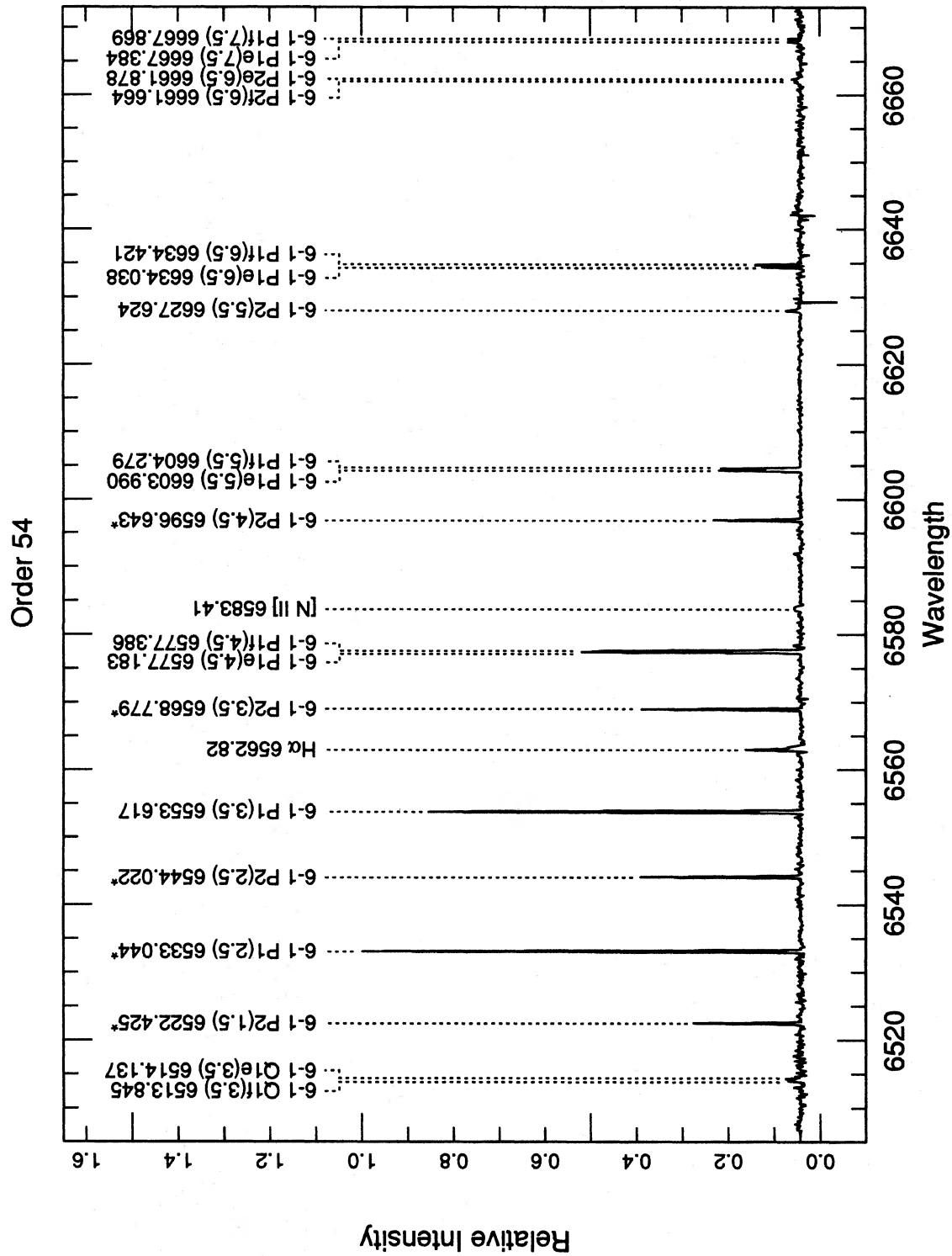

FIG. 11—Order 54 of Mauna Kea night-sky emission-line spectrum.

© Astronomical Society of the Pacific • Provided by the NASA Astrophysics Data System

1996PASP..108..277O

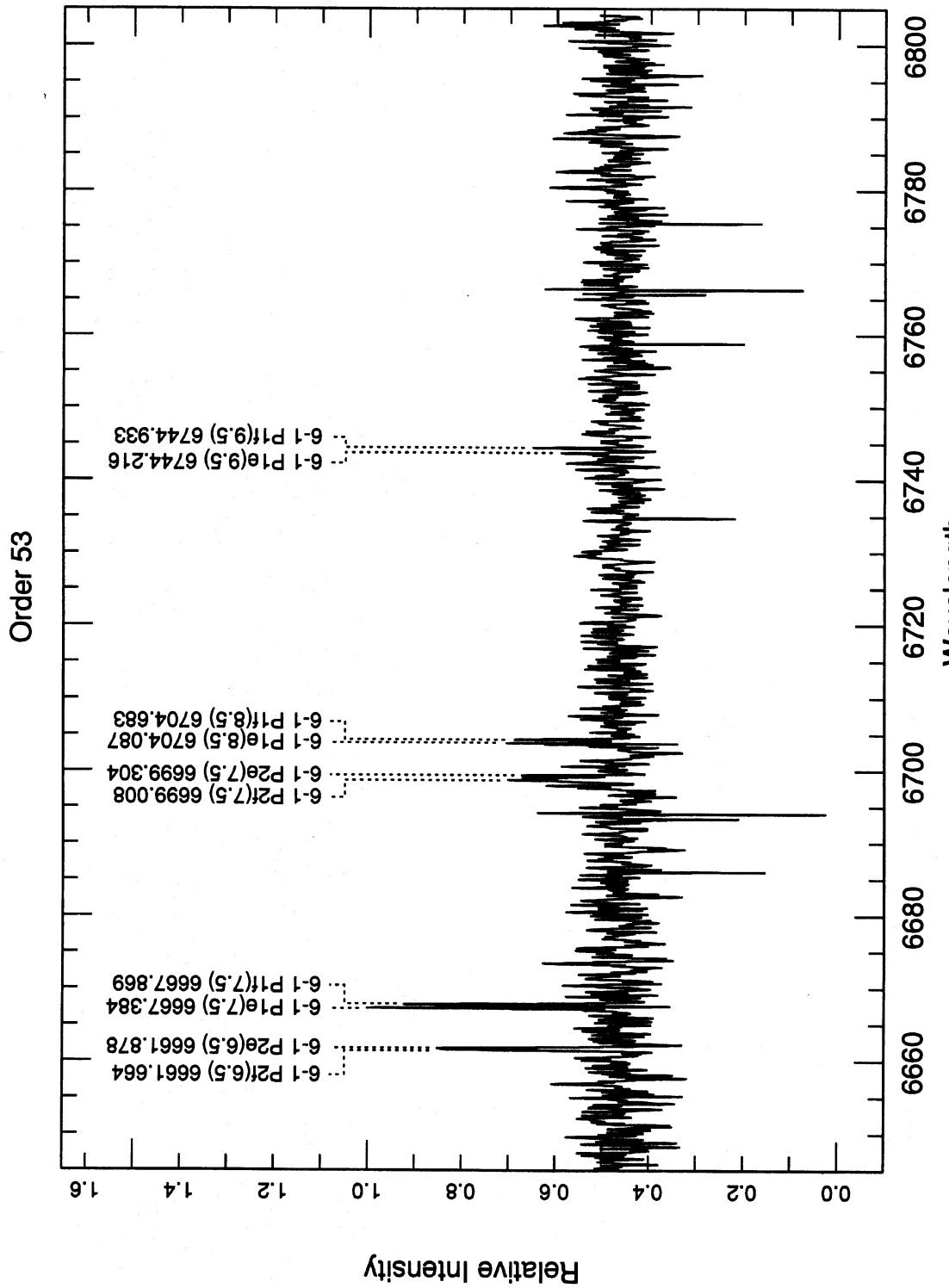

FIG. 12—Order 53 of Mauna Kea night-sky emission-line spectrum.

© Astronomical Society of the Pacific • Provided by the NASA Astrophysics Data System

1996PASP..108..2770

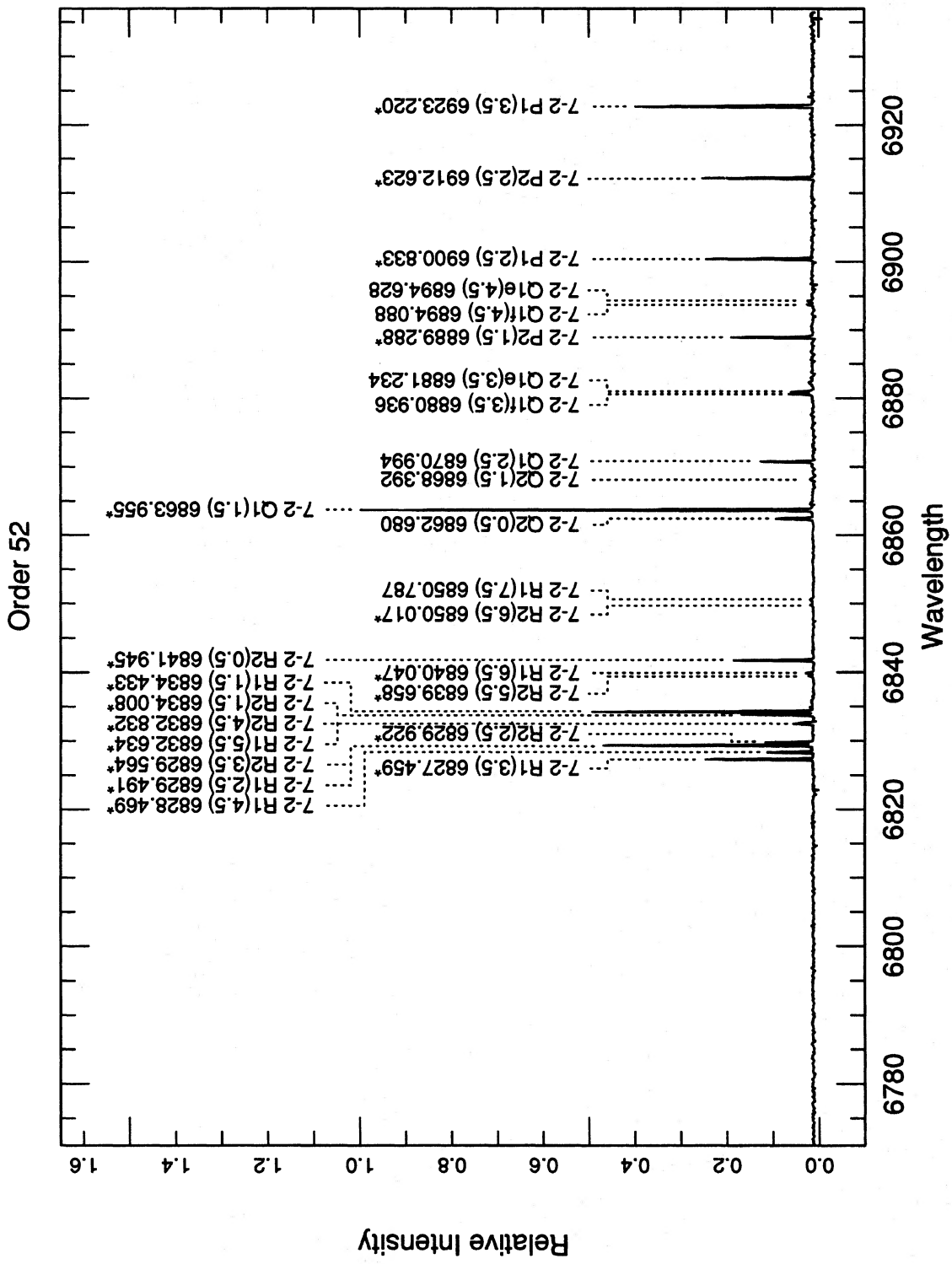

FIG. 13—Order 52 of Mauna Kea night-sky emission-line spectrum.

© Astronomical Society of the Pacific • Provided by the NASA Astrophysics Data System

1996PASP..108..2770

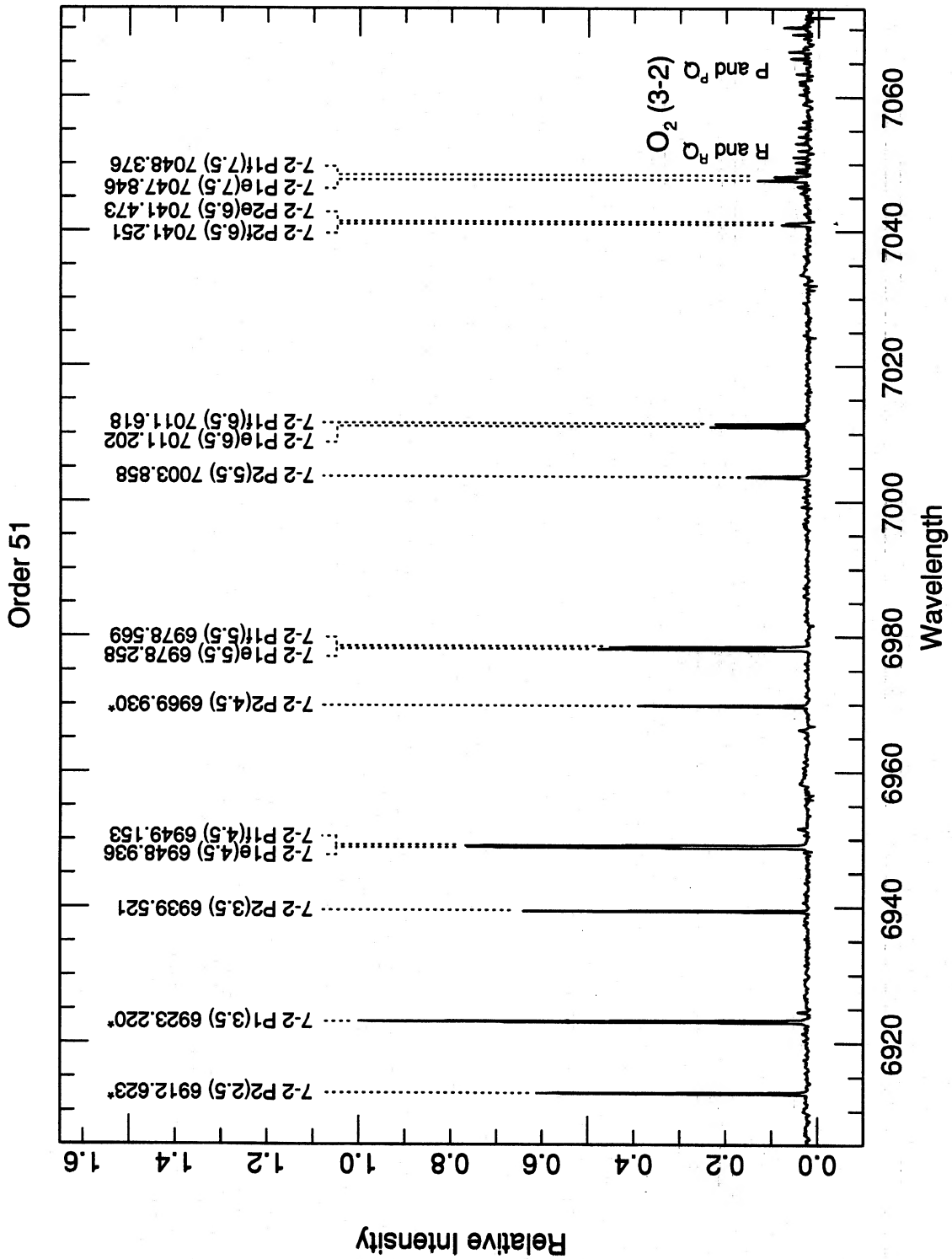

FIG. 14—Order 51 of Mauna Kea night-sky emission-line spectrum.

© Astronomical Society of the Pacific • Provided by the NASA Astrophysics Data System

1996PASP..108..277O

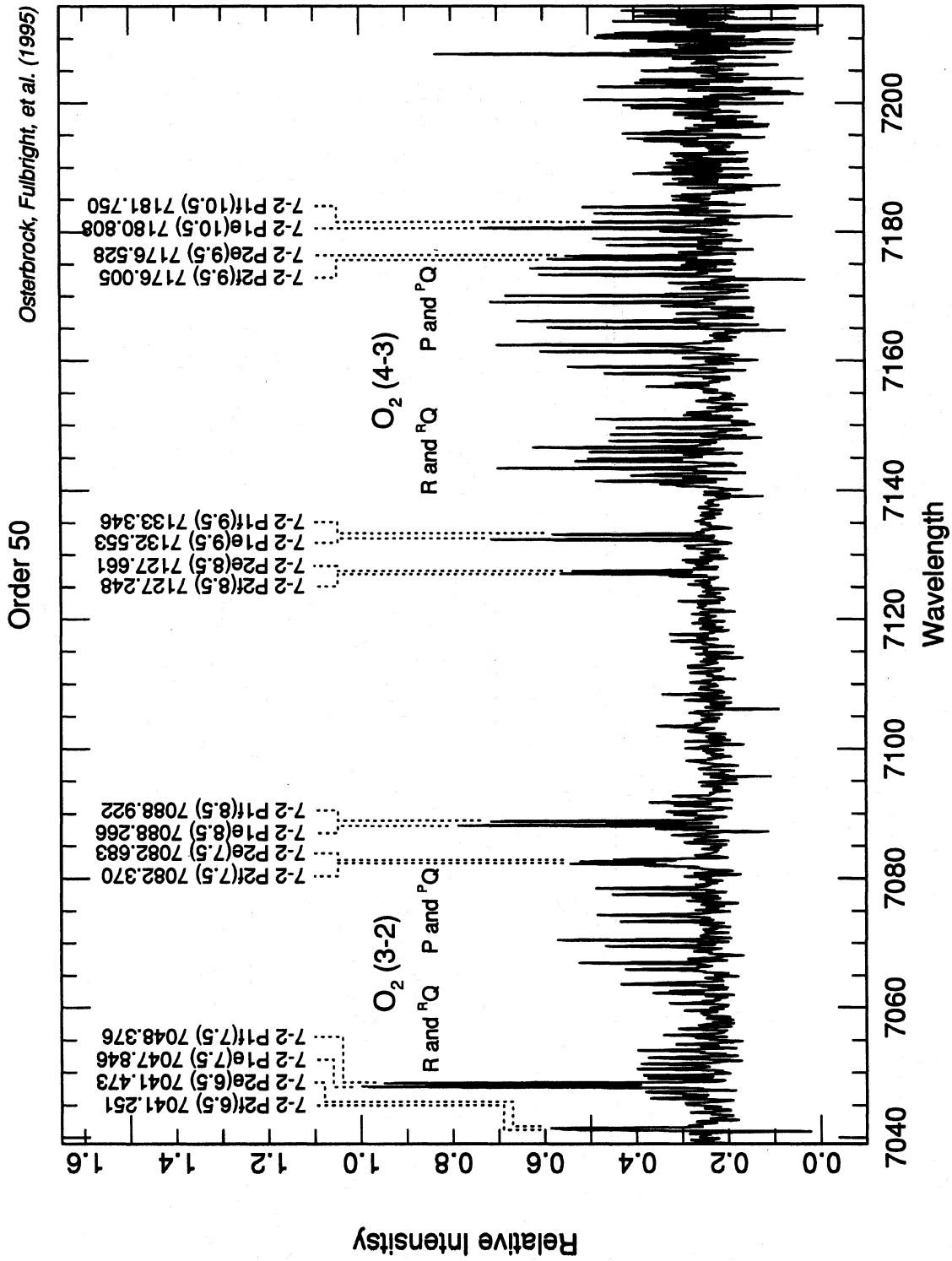

FIG. 15—Order 50 of Mauna Kea night-sky emission-line spectrum.

© Astronomical Society of the Pacific • Provided by the NASA Astrophysics Data System

1996PASP..108..277O

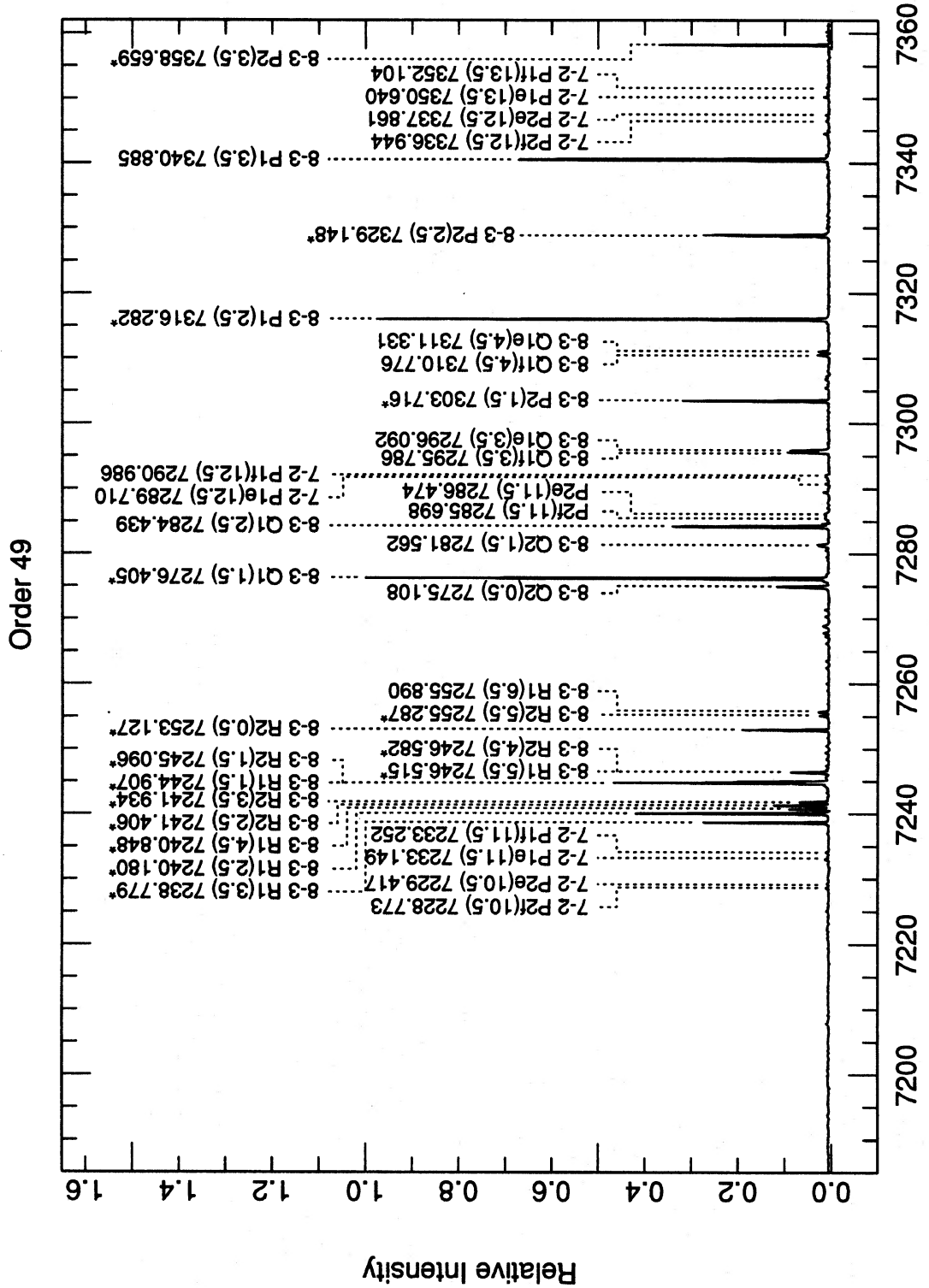

FIG. 16—Order 49 of Mauna Kea night-sky emission-line spectrum.

© Astronomical Society of the Pacific • Provided by the NASA Astrophysics Data System

1996PASP..108..277O

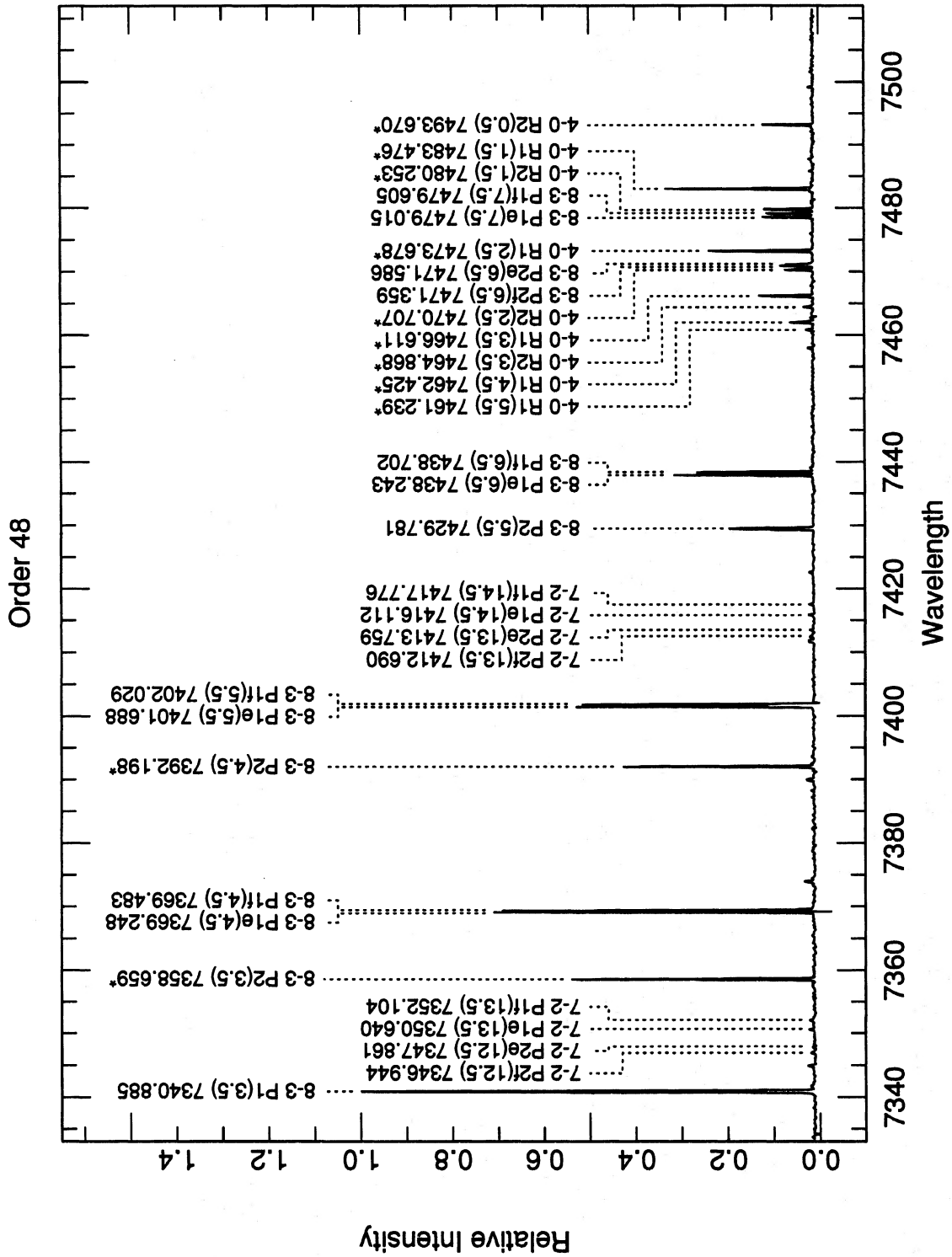

FIG. 17—Order 48 of Mauna Kea night-sky emission-line spectrum.

© Astronomical Society of the Pacific • Provided by the NASA Astrophysics Data System

1996PASP..108..2770

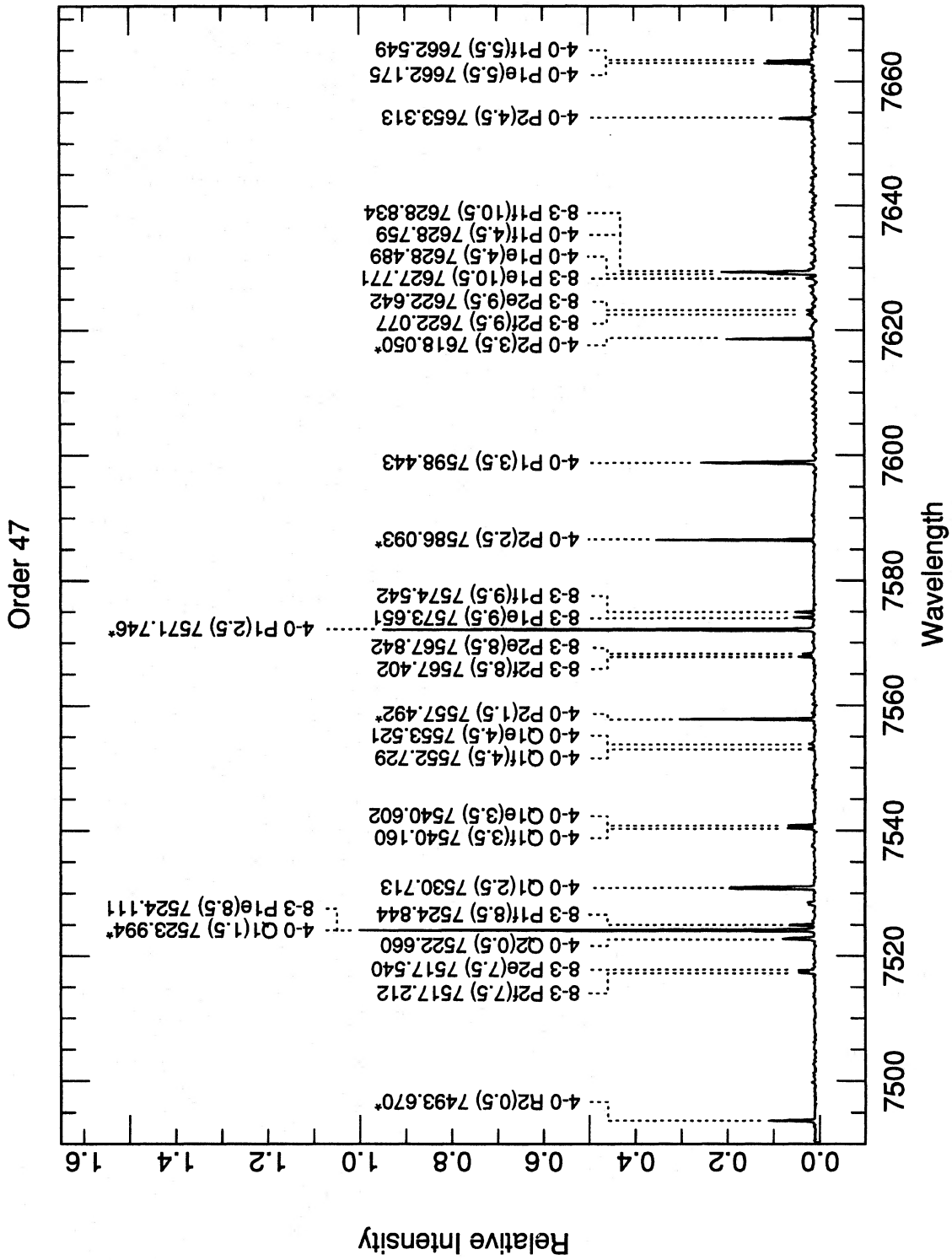

FIG. 18—Order 47 of Mauna Kea night-sky emission-line spectrum.

© Astronomical Society of the Pacific • Provided by the NASA Astrophysics Data System

1996PASP..108..277O

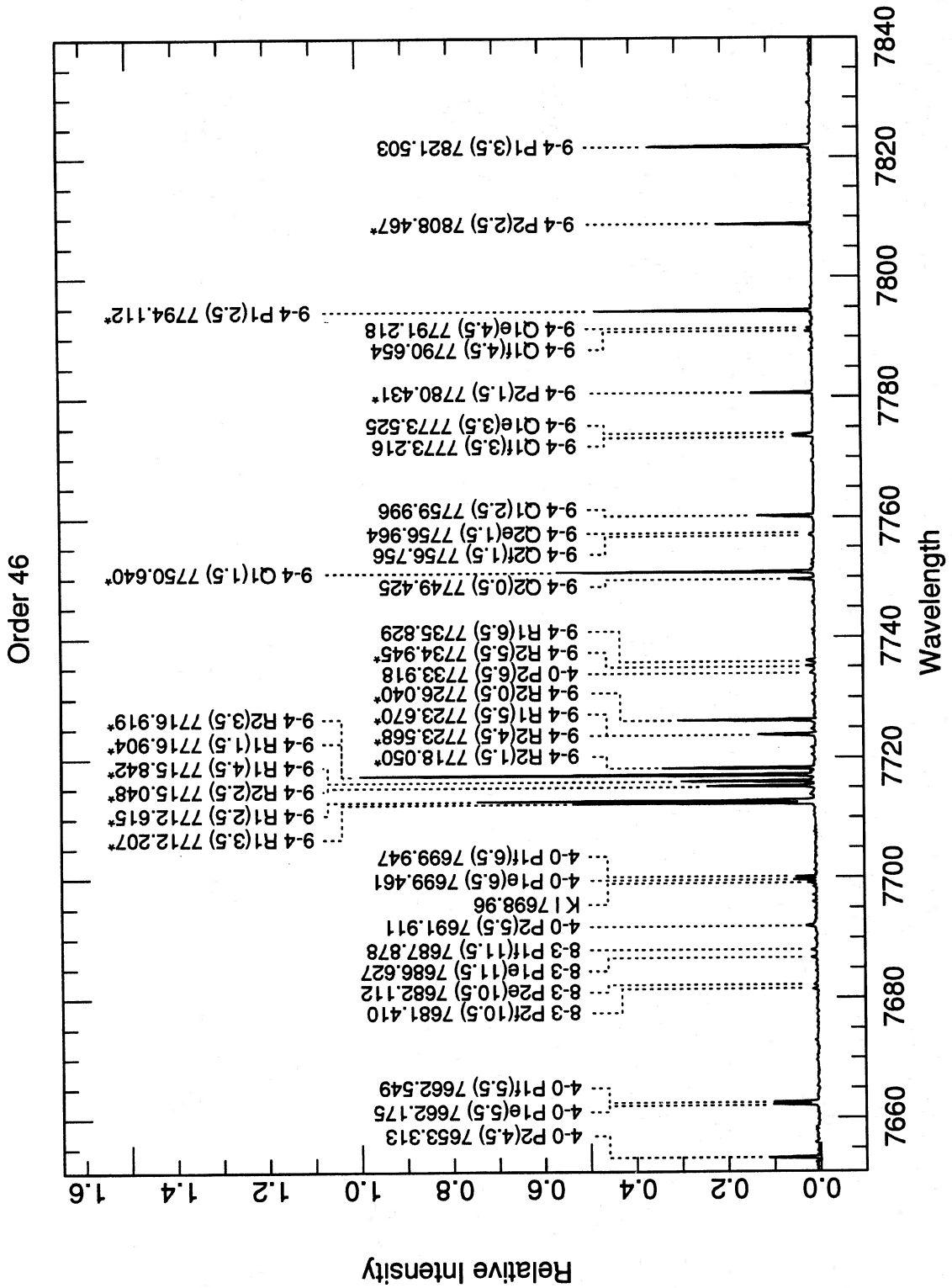

FIG. 19—Order 46 of Mauna Kea night-sky emission-line spectrum.

© Astronomical Society of the Pacific • Provided by the NASA Astrophysics Data System

1996PASP..108..277O

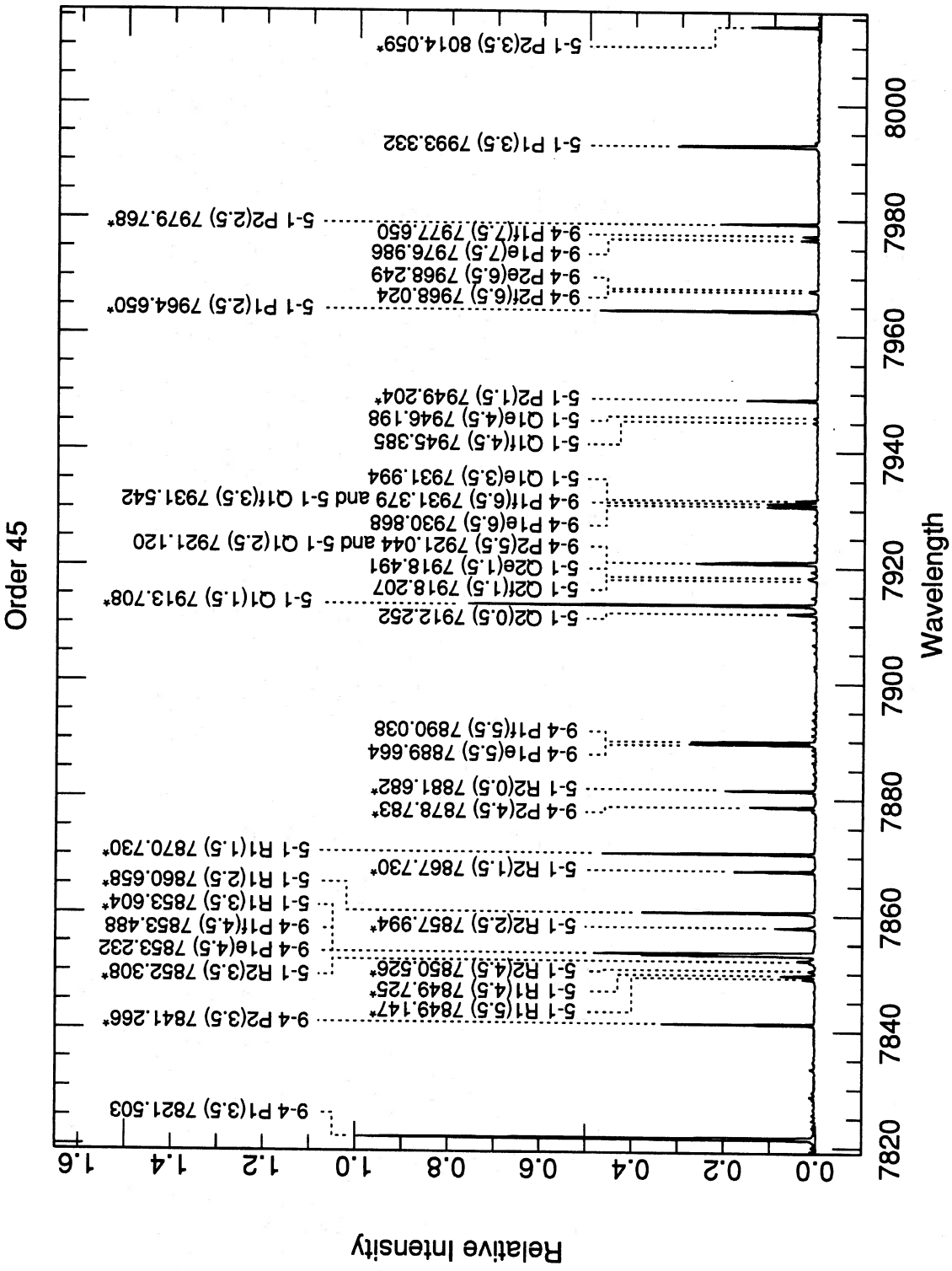

FIG. 20—Order 45 of Mauna Kea night-sky emission-line spectrum.

© Astronomical Society of the Pacific • Provided by the NASA Astrophysics Data System

1996PASP..108..277O

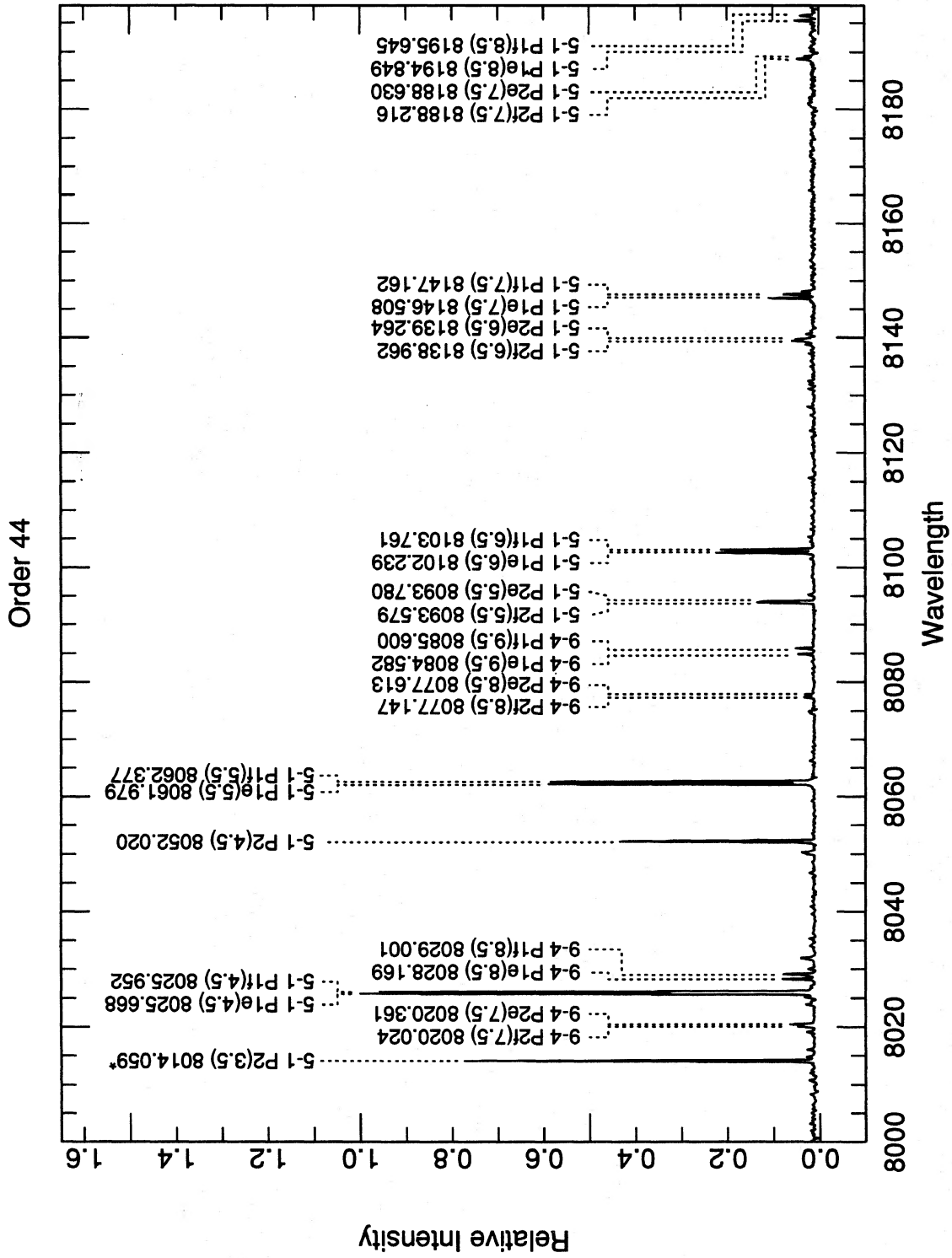

FIG. 21—Order 44 of Mauna Kea night-sky emission-line spectrum.

© Astronomical Society of the Pacific • Provided by the NASA Astrophysics Data System

1996PASP..108..277O

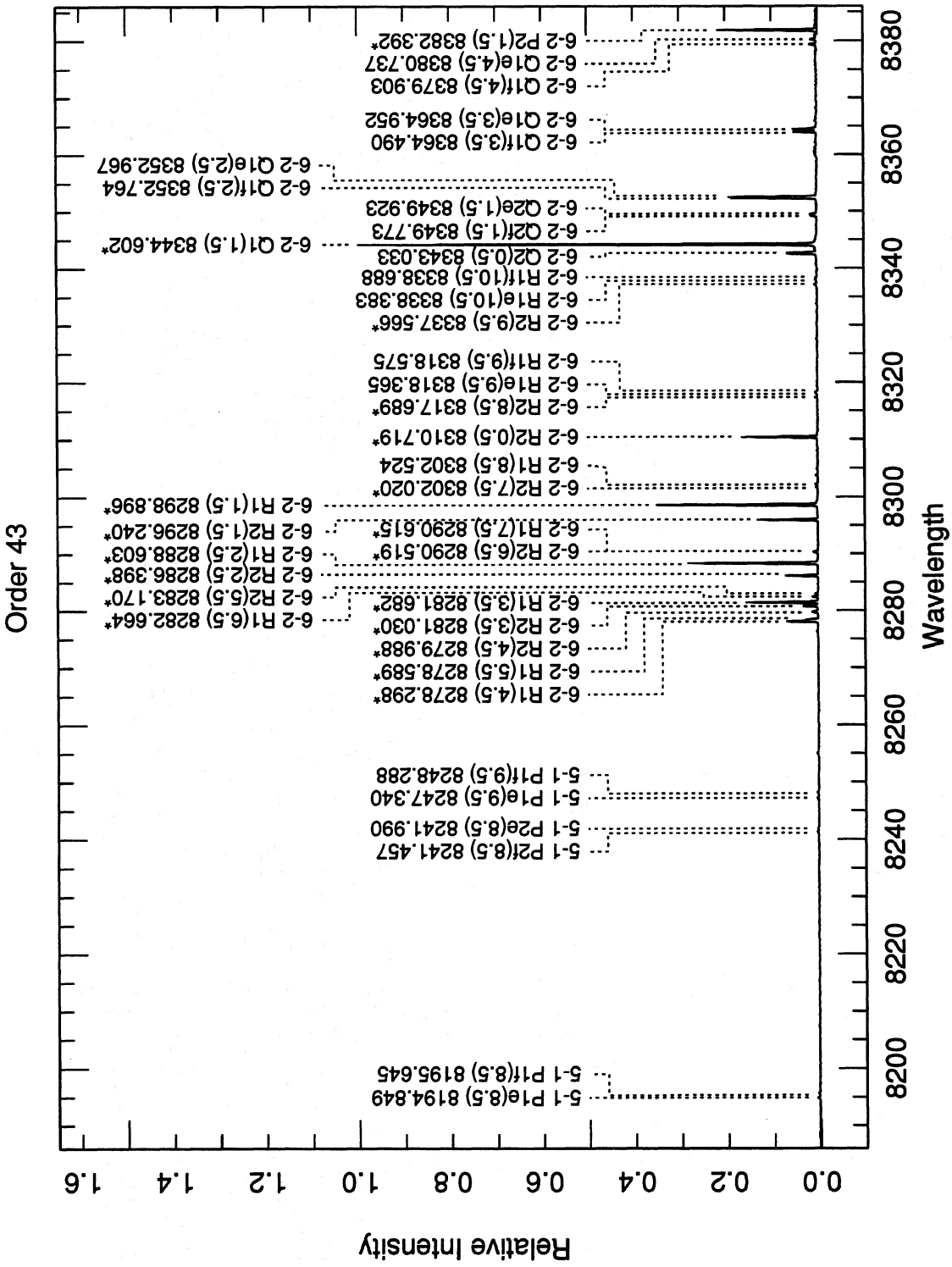

FIG. 22—Order 43 of Mauna Kea night-sky emission-line spectrum.

© Astronomical Society of the Pacific • Provided by the NASA Astrophysics Data System

1996PASP..108..277O

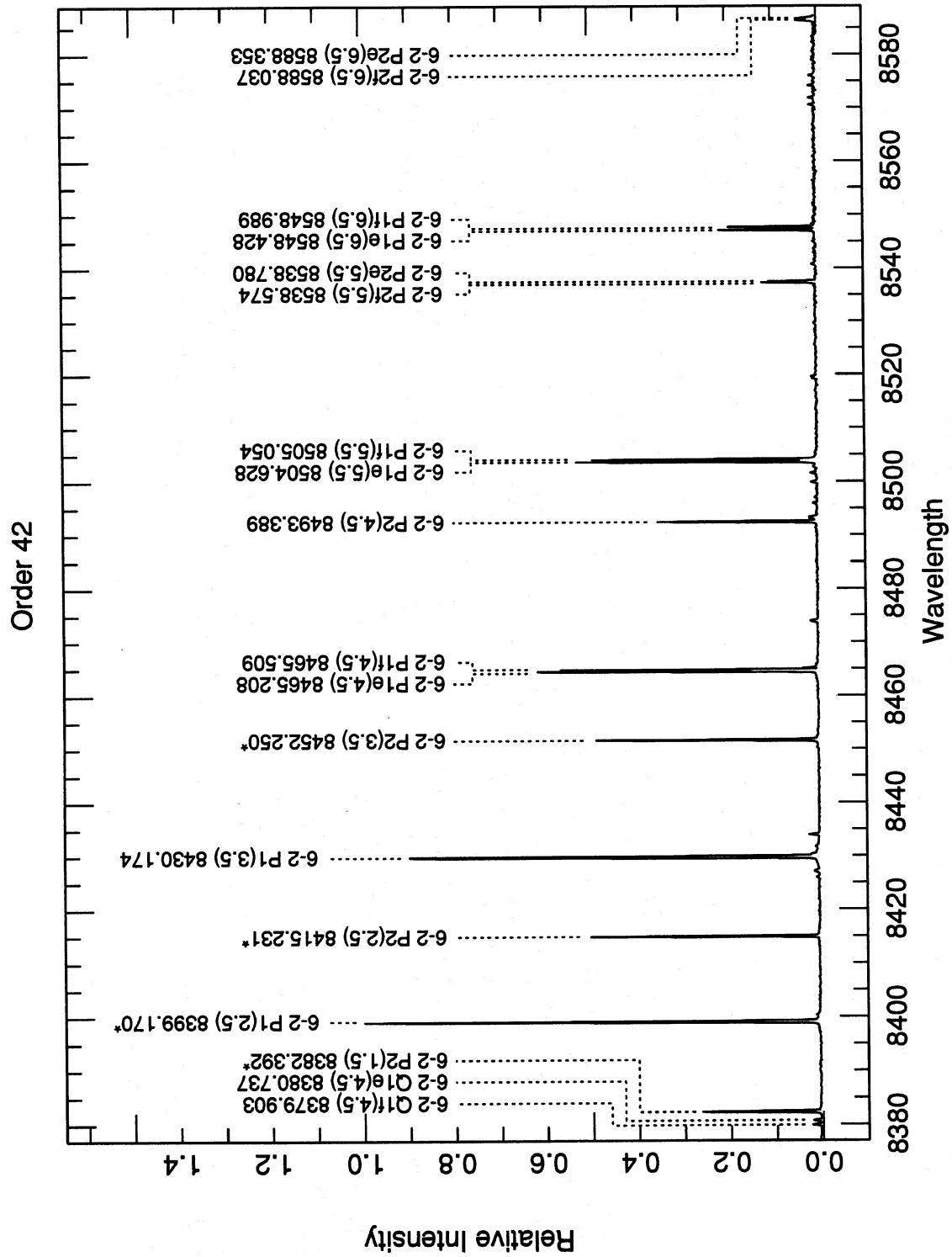

FIG. 23—Order 42 of Mauna Kea night-sky emission-line spectrum.

© Astronomical Society of the Pacific • Provided by the NASA Astrophysics Data System

1996PASP..108..277O

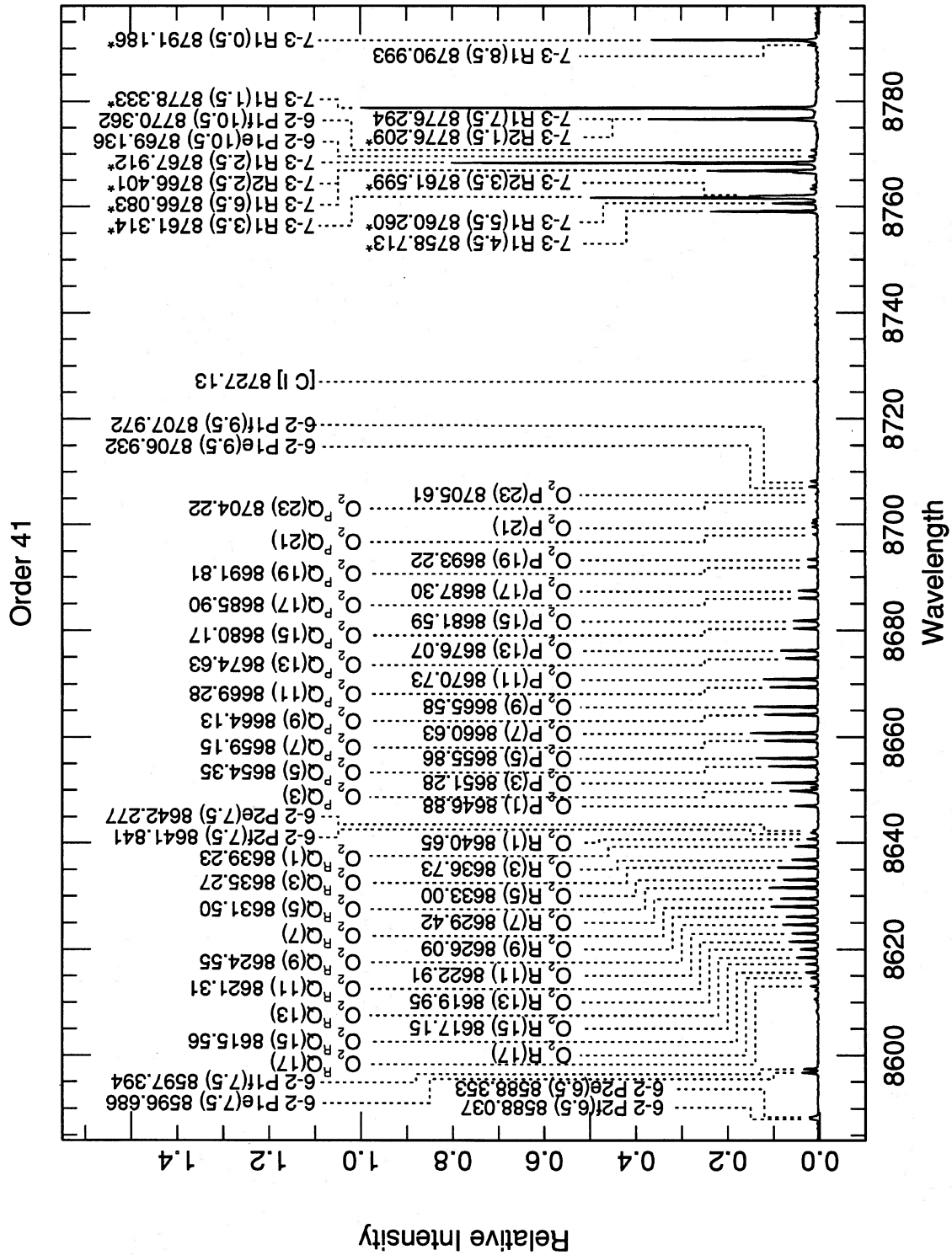

FIG. 24—Order 41 of Mauna Kea night-sky emission-line spectrum.

© Astronomical Society of the Pacific • Provided by the NASA Astrophysics Data System

1996PASP..108..2770

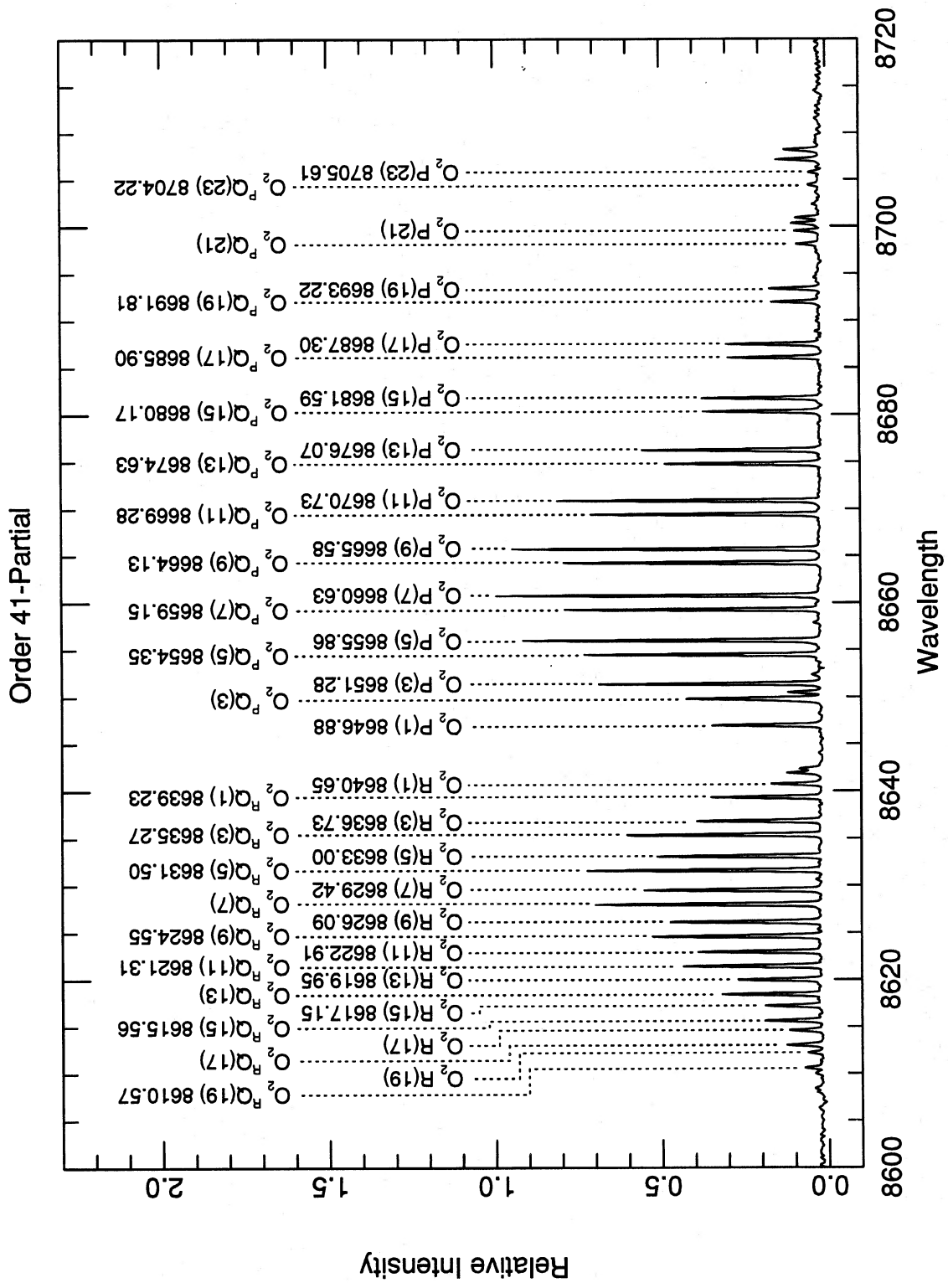

FIG. 25—Enlarged part of order 41 of Mauna Kea night-sky emission-line spectrum.

© Astronomical Society of the Pacific • Provided by the NASA Astrophysics Data System

1996PASP..108..277O

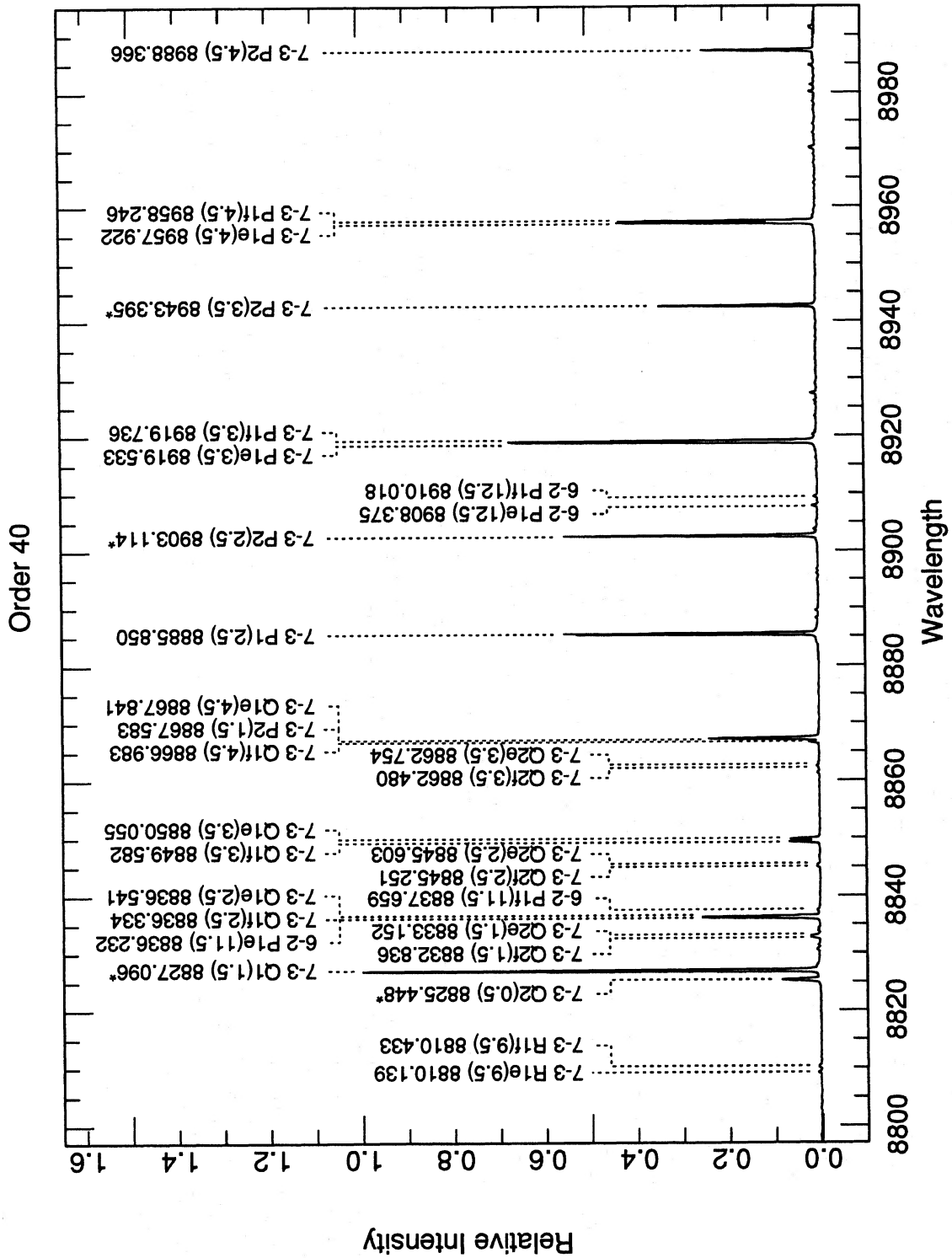

FIG. 26—Order 40 of Mauna Kea night-sky emission-line spectrum.

© Astronomical Society of the Pacific • Provided by the NASA Astrophysics Data System

1996PASP..108..2770

TABLE 2
Observed OH Lines Not Listed in Abrams et al. (1994)

v'-v"	Identification	Wavelength	v'-v"	Identification	Wavelength
7-1	P1e(5.5)	5645.158	6-1	R1f(4.5)	6463.793
7-1	P1f(5.5)	5645.386	6-1	R1e(4.5)	6463.810
7-1	P2f(5.5)	5664.130	6-1	P1e(5.5)	6603.990
7-1	P2e(5.5)	5664.231	6-1	P1f(5.5)	6604.279
8-2	P1e(5.5)	5976.953	6-1	P2f(5.5)	6627.555
8-2	P1f(5.5)	5977.200	6-1	P2e(5.5)	6627.693
8-2	P2f(5.5)	5997.715	6-1	P1e(6.5)	6634.038
8-2	P2e(5.5)	5997.814	6-1	P1f(6.5)	6634.421
8-2	P1e(6.5)	6003.744	6-1	P2f(6.5)	6661.664
8-2	P1f(6.5)	6004.078	6-1	P2e(6.5)	6661.878
8-2	P2f(6.5)	6028.353	6-1	P1e(7.5)	6667.384
8-2	P2e(6.5)	6028.518	6-1	P1f(7.5)	6667.869
8-2	P1e(7.5)	6033.783	6-1	P2f(7.5)	6699.008
8-2	P1f(7.5)	6034.214	6-1	P2e(7.5)	6699.304
8-2	P1e(8.5)	6067.147	6-1	P1e(8.5)	6704.087
8-2	P1f(8.5)	6068.684	6-1	P1f(8.5)	6704.683
5-0	R1f(4.5)	6136.541	6-1	P1e(9.5)	6744.216
5-0	R1e(4.5)	6136.566	6-1	P1f(9.5)	6744.933
5-0	R1f(5.5)	6138.859	6-1	P1e(10.5)	6787.849
5-0	R1e(5.5)	6138.863	6-1	P1f(10.5)	6788.697
9-3	R1e(4.5)	6240.176	7-2	R1f(4.5)	6828.466
9-3	R1f(4.5)	6240.219	7-2	R1e(4.5)	6828.473
9-3	R1e(5.5)	6247.957	7-2	R1e(5.5)	6832.621
9-3	R1f(5.5)	6248.047	7-2	R1f(5.5)	6832.648
5-0	P1e(5.5)	6268.270	7-2	R2e(4.5)	6832.803
5-0	P1f(5.5)	6268.540	7-2	R2f(4.5)	6832.860
9-3	P1e(5.5)	6356.167	7-2	R2e(5.5)	6839.635
9-3	P1f(5.5)	6356.441	7-2	R2f(5.5)	6839.681
9-3	P2f(5.5)	6379.268	7-2	R1e(6.5)	6840.011
9-3	P2e(5.5)	6379.361	7-2	R1f(6.5)	6840.082
9-3	P1e(6.5)	6386.236	7-2	R2e(6.5)	6850.005
9-3	P1f(6.5)	6386.424	7-2	R2f(6.5)	6850.028
9-3	P2f(6.5)	6413.720	7-2	R1e(7.5)	6850.722
9-3	P2e(6.5)	6413.885	7-2	R1f(7.5)	6850.851
9-3	P1e(7.5)	6420.056	7-2	P1e(5.5)	6978.258
9-3	P1f(7.5)	6420.544	7-2	P1f(5.5)	6978.569
9-3	P2f(7.5)	6451.960	7-2	P2f(5.5)	7003.788
9-3	P2e(7.5)	6452.209	7-2	P2e(5.5)	7003.928
9-3	P1e(8.5)	6457.734	7-2	P1e(6.5)	7011.202
9-3	P1f(8.5)	6458.344	7-2	P1f(6.5)	7011.618
7-2	P2f(6.5)	7041.251	7-2	P2f(13.5)	7412.690
7-2	P2e(6.5)	7041.473	7-2	P2e(13.5)	7413.759
7-2	P1e(7.5)	7047.846	7-2	P1e(14.5)	7416.112
7-2	P1f(7.5)	7048.376	7-2	P1f(14.5)	7417.776
7-2	P2f(7.5)	7082.370	8-3	P2f(5.5)	7429.712
7-2	P2e(7.5)	7082.683	8-3	P2e(5.5)	7429.849
7-2	P1e(8.5)	7088.266	8-3	P1e(6.5)	7438.243
7-2	P1f(8.5)	7088.922	8-3	P1f(6.5)	7438.702
7-2	P2f(8.5)	7127.248	4-0	R1f(5.5)	7461.206
7-2	P2e(8.5)	7127.661	4-0	R1e(5.5)	7461.271
7-2	P1e(9.5)	7132.553	4-0	R1f(4.5)	7462.385
7-2	P1f(9.5)	7133.346	4-0	R1e(4.5)	7462.464
7-2	P2f(9.5)	7176.005	8-3	P2f(6.5)	7471.359
7-2	P2e(9.5)	7176.528	8-3	P2e(6.5)	7471.586
7-2	P1e(10.5)	7180.808	8-3	P1e(7.5)	7479.015
7-2	P1f(10.5)	7181.750	8-3	P1f(7.5)	7479.605
7-2	P2f(10.5)	7228.773	8-3	P2f(7.5)	7517.212
7-2	P2e(10.5)	7229.417	8-3	P2e(7.5)	7517.540
7-2	P1e(11.5)	7233.149	8-3	P1e(8.5)	7524.111
7-2	P1f(11.5)	7233.252	8-3	P1f(8.5)	7524.844
8-3	R1e(4.5)	7240.843	8-3	P2f(8.5)	7567.402
8-3	R1f(4.5)	7240.854	8-3	P2e(8.5)	7567.842
8-3	R1e(5.5)	7246.488	8-3	P1e(9.5)	7573.651
8-3	R1f(5.5)	7246.542	8-3	P1f(9.5)	7574.542
8-3	R2e(4.5)	7246.548	8-3	P2f(9.5)	7622.077
8-3	R2f(4.5)	7246.615	8-3	P2e(9.5)	7622.642
8-3	R2e(5.5)	7255.261	8-3	P1e(10.5)	7627.771
8-3	R2f(5.5)	7255.312	8-3	P1f(10.5)	7628.834
8-3	R1e(6.5)	7255.835	4-0	P1e(5.5)	7662.175
8-3	R1f(6.5)	7255.945	4-0	P1f(5.5)	7662.549
7-2	P2f(11.5)	7285.698	8-3	P2f(10.5)	7681.410
7-2	P2e(11.5)	7286.474	8-3	P2e(10.5)	7682.112
7-2	P1e(12.5)	7289.710	8-3	P1e(11.5)	7686.627
7-2	P1f(12.5)	7290.986	8-3	P1f(11.5)	7687.878
7-2	P2f(12.5)	7346.944	4-0	P2f(5.5)	7691.813
7-2	P2e(12.5)	7347.861	4-0	P2e(5.5)	7692.009
7-2	P1e(13.5)	7350.640	4-0	P1e(6.5)	7699.461
7-2	P1f(13.5)	7352.104	4-0	P1f(6.5)	7699.947
8-3	P1e(5.5)	7401.688	9-4	R1e(4.5)	7715.824
8-3	P1f(5.5)	7402.029	9-4	R1f(4.5)	7715.859

nents labeled separately and a blend labeled as a single line. Furthermore if the two lines are separated by 0.1 Å or less, the mean wavelength is marked with an asterisk on the figures. Thus, for wavelength calibration, the best lines to use are the single lines marked with an *e* or *f*. Their wavelengths are known exactly. The next best are the blends with separation less than 0.1 Å, whose wavelengths are marked with an asterisk. Their mean wavelengths could be very slightly in error, if the *e* and *f* components differ greatly in intensity. The least desirable lines to use are the blends with separation between 0.1 and 0.2 Å, which are not marked with an *e* or *f* nor with an asterisk. Since their separations are larger, the error in their mean wavelengths could be proportionately larger. But any such errors appear to be well below 0.01 Å. One additional potential problem with using the OH lines for wavelength calibration can occur near the *R* band heads. There the separations between successive J lines become small and change sign, so that two lines of different J and different intensity may be blended. We have tried to mark these cases on the figures, and unless the lines can be seen resolved, these blends should be avoided.

In their Table 29, Abrams et al. (1994) list wavelengths of the P(J) and Q(J) lines with $J \leq 4.5$, and of $R(J)$ with $J \leq 3.5$. However, lines of higher J can easily be seen in many observed bands of the night-sky spectrum. The rotational term values (energy levels in cm^{-1}) of all the levels deduced from laboratory data by Abrams et al. (1994) are listed in their Table 27, and from them we have calculated the wavelengths of all the OH lines with J larger than those limits, which we have identified in our spectra. These calculated wavelengths were converted from vacuum to air using the dispersion formula for standard air published by Edlén (1953), which is the one Abrams et al. (1994) actually used, although they state they used the later determination, also by Edlén (1966). We reproduce their tabulated wavelengths to 0.00001 Å, the last figure tabulated in their paper, by using Edlén (1953), but find discrepancies of order 0.0001 Å using Edlén (1966). These lines of higher J are especially useful for wavelength calibration, because of the large Λ-type splitting and the consequent resolution of the two components of the lines.

For completeness, these calculated wavelengths for the higher rotational lines observed in the night-sky spectrum with the Keck HIRES are listed in Table 2. They are entered on the figures as described above, in just the same way as the wavelengths listed by Abrams et al. for the lower rotational levels.

4. O_2 BANDS

There is also an O_2 band in the region λλ8610–8685, which is completely unresolved at low dispersion, but beau-

© Astronomical Society of the Pacific • Provided by the NASA Astrophysics Data System

1996PASP..108..277O

TABLE 2
(Continued)

v'-v"	Identification	Wavelength	v'-v"	Identification	Wavelength
9-4	R2e(4.5)	7723.525	5-1	P2f(6.5)	8138.962
9-4	R2f(4.5)	7723.611	5-1	P2e(6.5)	8139.264
9-4	R1e(5.5)	7723.625	5-1	P1e(7.5)	8146.508
9-4	R1f(5.5)	7723.715	5-1	P1f(7.5)	8147.162
4-0	P2f(6.5)	7733.773	5-1	P2f(7.5)	8188.216
4-0	P2e(6.5)	7734.063	5-1	P2e(7.5)	8188.630
9-4	R2e(5.5)	7734.913	5-1	P1e(8.5)	8194.849
9-4	R2f(5.5)	7734.978	5-1	P1f(8.5)	8195.645
9-4	R1e(6.5)	7735.747	5-1	P2f(8.5)	8241.457
9-4	R1f(6.5)	7735.910	5-1	P2e(8.5)	8241.990
5-1	R1f(5.5)	7849.120	5-1	P1e(9.5)	8247.340
5-1	R1e(5.5)	7849.173	5-1	P1f(9.5)	8248.288
5-1	R1f(4.5)	7849.689	6-2	R1f(4.5)	8278.267
5-1	R1e(4.5)	7849.761	6-2	R1e(4.5)	8278.330
5-1	R2e(4.5)	7850.479	6-2	R1f(5.5)	8278.570
5-1	R2f(4.5)	7850.573	6-2	R1e(5.5)	8278.607
9-4	P1e(5.5)	7889.664	6-2	R2e(4.5)	8279.940
9-4	P1f(5.5)	7890.038	6-2	R2f(4.5)	8280.037
9-4	P2f(5.5)	7920.982	6-2	R1e(6.5)	8282.662
9-4	P2e(5.5)	7921.106	6-2	R1f(6.5)	8282.665
9-4	P1e(6.5)	7930.868	6-2	R2e(5.5)	8283.122
9-4	P1f(6.5)	7931.379	6-2	R2f(5.5)	8283.217
9-4	P2f(6.5)	7968.024	6-2	R2e(6.5)	8290.479
9-4	P2e(6.5)	7968.249	6-2	R2f(6.5)	8290.558
9-4	P1e(7.5)	7976.986	6-2	R1e(7.5)	8290.585
9-4	P1f(7.5)	7977.650	6-2	R1f(7.5)	8290.644
9-4	P2f(7.5)	8020.024	5-1	P2f(9.5)	8298.809
9-4	P2e(7.5)	8020.361	5-1	P2e(9.5)	8299.471
9-4	P1e(8.5)	8028.169	6-2	R2e(7.5)	8301.995
9-4	P1f(8.5)	8029.001	6-2	R2f(7.5)	8302.045
5-1	P1e(5.5)	8061.979	6-2	R1e(8.5)	8302.460
5-1	P1f(5.5)	8062.377	6-2	R1f(8.5)	8302.587
9-4	P2f(8.5)	8077.147	5-1	P1e(10.5)	8304.071
9-4	P2e(8.5)	8077.613	5-1	P1f(10.5)	8305.184
9-4	P1e(9.5)	8084.582	6-2	R2e(8.5)	8317.685
9-4	P1f(9.5)	8085.600	6-2	R2f(8.5)	8317.693
5-1	P2f(5.5)	8093.579	6-2	R1e(9.5)	8318.365
5-1	P2e(5.5)	8093.780	6-2	R1f(9.5)	8318.575
5-1	P1e(6.5)	8102.239	6-2	R2f(9.5)	8337.544
5-1	P1f(6.5)	8103.761	6-2	R2e(9.5)	8337.589
6-2	R1e(10.5)	8338.383	5-1	P2f(15.5)	8737.466
6-2	R1f(10.5)	8338.688	5-1	P2e(15.5)	8739.107
5-1	P2f(10.5)	8360.404	5-1	P1e(16.5)	8740.603
5-1	P2e(10.5)	8361.206	5-1	P1f(16.5)	8742.913
5-1	P1e(11.5)	8365.150	7-3	R1f(4.5)	8758.690
5-1	P1f(11.5)	8366.437	7-3	R1e(4.5)	8758.736
5-1	P2f(11.5)	8426.386	7-3	R1f(5.5)	8760.255
5-1	P2e(11.5)	8427.338	7-3	R1e(5.5)	8760.265
5-1	P1e(12.5)	8430.698	6-2	P2f(9.5)	8763.017
5-1	P1f(12.5)	8432.171	6-2	P2e(9.5)	8763.725
5-1	P2f(12.5)	8496.908	7-3	R1e(6.5)	8766.062
5-1	P2e(12.5)	8498.020	7-3	R1f(6.5)	8766.105
5-1	P1e(13.5)	8500.853	6-2	P1e(10.5)	8769.136
5-1	P1f(13.5)	8502.523	6-2	P1f(10.5)	8770.362
6-2	P1e(5.5)	8504.628	7-3	R1e(7.5)	8776.238
6-2	P1f(5.5)	8505.054	7-3	R1f(7.5)	8776.349
6-2	P2f(5.5)	8538.574	7-3	R1e(8.5)	8790.896
6-2	P2e(5.5)	8538.780	7-3	R1f(8.5)	8791.091
6-2	P1e(6.5)	8548.428	7-3	R1e(9.5)	8810.139
6-2	P1f(6.5)	8548.989	7-3	R1f(9.5)	8810.433
5-1	P2f(13.5)	8572.138	6-2	P2f(10.5)	8830.698
5-1	P2e(13.5)	8573.419	5-1	P1e(17.5)	8830.922
5-1	P1e(14.5)	8575.771	6-2	P2e(10.5)	8831.559
5-1	P1f(14.5)	8577.647	5-1	P1f(17.5)	8833.454
6-2	P2f(6.5)	8588.037	6-2	P1e(11.5)	8836.232
6-2	P2e(6.5)	8588.353	6-2	P1f(11.5)	8837.659
6-2	P1e(7.5)	8596.686	6-2	P2f(11.5)	8903.336
6-2	P1f(7.5)	8597.394	6-2	P2e(11.5)	8904.363
6-2	P2f(7.5)	8641.841	6-2	P1e(12.5)	8908.375
6-2	P2e(7.5)	8642.277	6-2	P1f(12.5)	8910.018
6-2	P1e(8.5)	8949.487	5-1	P1e(18.5)	8926.817
6-2	P1f(8.5)	8950.355	5-1	P1f(18.5)	8929.566
5-1	P2f(14.5)	8652.257	6-2	P2f(12.5)	8981.124
5-1	P2e(14.5)	8653.716	6-2	P2e(12.5)	8982.327
5-1	P1e(15.5)	8655.624	6-2	P1e(13.5)	8985.739
5-1	P1f(15.5)	8657.714	6-2	P1f(13.5)	8987.611
6-2	P2f(8.5)	8700.118			
6-2	P2e(8.5)	8700.685			
6-2	P1e(9.5)	8706.932			
6-2	P1f(9.5)	8707.972			

tifully resolved with HIRES, as shown in Fig. 25. Identified by Meinel (1950b), it is the (0–1) band of the $b^1\Sigma^+ - X^3\Sigma^-$ "red" atmospheric system. We have not been able to find published wavelengths for its individual lines, but it is straightforward to calculate them from combination differences formed from wavelengths of other bands of this system, measured accurately as absorption lines arising in the Earth's atmosphere in the solar spectrum (Babcock and Herzberg 1948). In this forbidden electronic transition, the lower $^3\Sigma^-$ electronic term has $\Lambda=0$ and $\Sigma=1$, and it is well described by Hund's case (b). The total angular momentum apart from spin $K''=1,3,5,...$ (only odd K levels exist because of the symmetry properties of the electronic wave function and the two identical O^{16} nuclei), and each of these rotational levels is further split into three levels with total angular momentum $J''=K''-1$, K'', and $K''+1$. The atmospheric bands occur by magnetic-dipole transitions between these levels and the levels of the upper $^1\Sigma^+$ term, which have $J'=K'=0,2,4,...$ only. The result of the selection rules is that the (0–1) band, and all the other rotation–vibration bands of this system, have four branches, called $R(J')$, $^RQ(J'')$, $^PQ(J'')$, and $P(J'')$. The symbols on the line have the same meaning as for OH, without a superscript if $(K'-K'')=(J'-J'')$, but with superscript R or P before the Q if $(K'-K'')=1$ or -1, respectively.

Telluric lines of the (0–0), (1–0), (2–0), (3–0), (1–1), (2–1), and (3–1) bands of this O_2 system were all observed in absorption in the solar spectrum with high-dispersion by Babcock and Herzberg (1948), who published accurate measured wavelengths of them. The (2–1) and (3–1) bands are the weakest, and the (0–1) band could not be seen in absorption. However, the wavelengths of the lines in the latter band can easily be calculated from the combination differences of the vacuum wave numbers of the same rotational lines in three other bands which they did measure, one with $v'=0$, and two with $v'=1,2$, or 3

$$\nu(0-1)=\nu(0-0)-\nu(v'-0)+\nu(v'-1).$$

These wave numbers were converted to air wavelengths using the same formula as for the OH lines (Edlén 1953). The lines in the (1–0) and (1–1) bands (with $v'=1$) are the strongest and best measured; the wavelengths of the lines in the (0–1) band calculated from them are listed in Table 3. Only lines for which all three wave numbers needed for the calculation were measured as unblended by Babcock and Herzberg (1948) are listed. The wavelengths of a few lines in

© Astronomical Society of the Pacific • Provided by the NASA Astrophysics Data System

1996PASP..108..277O

TABLE 3
Calculated Wavelengths for O_2 (0-1)

Identification	Calculated λ	Identification	Calculated λ
$^RQ(21)$	—	P(1)	8646.88
R(21)	8609.98	$^PQ(3)$	—
$^RQ(19)$	8610.57	P(3)	8651.28
R(19)	—	$^PQ(5)$	8654.35
$^RQ(17)$	—	P(5)	8655.86
R(17)	—	$^PQ(7)$	8659.15
$^RQ(15)$	8615.56	P(7)	8660.63
R(15)	8617.15	$^PQ(9)$	8664.13
$^RQ(13)$	—	P(9)	8665.58
R(13)	8619.95	$^PQ(11)$	8669.28
$^RQ(11)$	8621.31	P(11)	8670.73
R(11)	8622.91	$^PQ(13)$	8674.63
$^RQ(9)$	8624.55	P(13)	8676.07
R(9)	8626.09	$^PQ(15)$	8680.17
$^RQ(7)$	—	P(15)	8681.59
R(7)	8629.42	$^PQ(17)$	8685.90
$^RQ(5)$	8631.50	P(17)	8687.30
R(5)	8633.00	$^PQ(19)$	8691.81
$^RQ(3)$	8635.27	P(19)	8693.22
R(3)	8636.73	$^PQ(21)$	—
$^RQ(1)$	8639.23	P(21)	—
R(1)	8640.65	$^PQ(23)$	8704.22
		P(23)	8705.61

this band can also be calculated from the weaker lines with $v'=2$; they agree with those from $v'=1$ to better than 0.01 Å. Wavelength measurements on our spectra, either with respect to the OH lines, or with the other O_2 lines, confirm this estimate of the accuracy. The wavelengths for the lines in the (0–1) band calculated from the still weaker $v'=3$ bands show considerably larger scatter, up to ±0.2 Å in some cases, probably indicating that the lines of these bands were in fact too weak to measure accurately. The (0–1) band is shown in Fig. 24, and also, at smaller scale, in Fig. 23 of the entire order 41.

Several other weaker bands of the same O_2 system can be seen in the HIRES night-sky spectrum. They are the (3–2) and (4–3) bands of the $\Delta v=+1$ sequence, in the wavelength ranges λλ7043–7086 and λλ7141–7185, and probably also the (5–4) band in the range λλ7240–7280. The identifications of the (3–2) and (4–3) bands are confirmed by their close agreement with a synthetic spectrum of O_2 in this region kindly calculated for us by Dr. D. B. Hatfield, using an assumed rotational temperature $T=300$ K (Johnstone et al. 1994). These two bands are marked on Fig. 15 (order 50), but the wavelengths of their lines are not known for high accuracy, so they cannot be used for wavelength calibration. In addition, the (3–3) band of the $\Delta v=0$ sequence is probably also weakly present in the range λλ7880–7936, as well as the (4–4) band still more weakly, at λλ7987–8042. However, strong OH features make it difficult to be certain of the latter two O_2 bands. All of these O_2 bands have been observed in emission at low dispersion in the laboratory, but we are not aware of a previously published report of any of them in the night-sky spectrum (Herman et al. 1961, Krupenie 1972).

5. OTHER LINES

A few other lines are visible in these night-sky spectra. The well-known [O I] λλ5577, 6300, 6363 night-sky lines

TABLE 4
Wavelengths of Atomic Night-Sky Lines

Ion	Wavelength
[O I]	5577.34
Na I	5889.953
Na I	5895.923
[O I]	6300.30
[O I]	6363.78

are all present, and provide good wavelength calibration lines. Their intensities with respect to the OH lines vary from exposure to exposure, no doubt depending to some extent on the level of weak auroral activity at this low-latitude site. Mauna Kea is a very dark-sky location, and we see no sign of light pollution. Hg I λλ5461, 5770, 5791, ubiquitous in any populated part of the continental United States, are not present at all in the Mauna Kea HIRES sky spectra. Narrow Na I D λλ5890, 5896 are present, without any sign of the very broad component which arises in high-pressure sodium lamps, nor of the many other narrow Na I emission lines which accompany the D lines in low-pressure sodium lamps and in the night-sky spectrum at Mount Hamilton (Osterbrock, et al. 1976). The wavelengths of these atomic lines, collected from Moore (1945) and Kaufman and Sugar (1986) are listed in Table 4 for convenience.

Hα and [N II] λ6583 show very weakly in this spectrum, probably from faint diffuse interstellar-gas emission at high latitudes in the Galaxy (Reynolds 1990). It would be dangerous to use them for wavelength calibration without knowing the velocity of the emitting gas. Weak [C I] λ8727.13 (Liu et al. 1995) also appears to be present, perhaps from volcanic ash in the atmosphere. Very weak K I, probably natural and analogous to natural Na I (which apparently arises from NaCl from the oceans, carried up to 50 km altitude in the atmosphere) may possibly be present, but probably is not. What could be its weaker resonance line is present at λ7698.98, but there is no trace of λ7664.91, the other, stronger resonance line of this ion. There is no sign of Li I λλ6707.74, 6707.89, but a blend of the two OH lines $P_{1e}(8.5)$ and $P_{1f}(8.5)$ λλ6704.09, 6704.68 could conceivably be misinterpreted as a blend of these two Li I resonance lines at low dispersion.

6. CONCLUSION

For convenience of use, the tables and figures from this paper will be available via the WWW (http://ucowww.ucsc.edu/~jfulb/OH.html). The figures will be available in PostScript form, while the tables will be available in PostScript, Latex, and ASCII form. There will also be a supplemental table which expands Table 2 to include the wavelengths of the lines already published by Abrams et al. (1994).

We are most grateful to Thomas A. Barlow, Christopher Churchill, Geoffrey W. Marcy, W. L. W. Sargent, and Donna S. Womble for providing most of the observed spectra on which this atlas is based, and to D. Brooke Hatfield for cal-

© Astronomical Society of the Pacific • Provided by the NASA Astrophysics Data System

1996PASP..108..277O

culating the synthetic spectrum of O_2 in the λλ7000–7200 region. We are also grateful to Steven S. Vogt and Joseph S. Miller for their encouragement and assistance in getting this program started. Finally, we wish to thank the National Science Foundation for partial support of this research under Grant No. AST 91-23547.

REFERENCES

Abrams, M. C., Davis, S. P., Rao, M. L. P., Engleman, Jr., R., and Brault, J. W. 1994, ApJS, 93, 351
Babcock, H. D., and Herzberg, L. 1948, ApJ, 108, 167
Chamberlain, J. W. 1961, Physics of the Aurora and Airglow (New York, Academic)
Edlén, B. 1953, JOSA, 43, 339
Edlén, B. 1966, Metrologia, 2, 71
Herman, L., Herman, R., and Rakotoarijimy, D. 1961, J. Physique, 22, 1
Herzberg, G. 1950, Molecular Spectra and Molecular Structure. I. Spectra of Diatomic Molecules (New York, Van Nostrand)
Johnstone, J. E., Hatfield, D. B., and Broadfoot, A. L. 1994, SPIE Conference 2226, 480
Kaufman, V., and Sugar, J. 1986, J. Phys. Chem. Ref. Data, 15, 321
Krupenie, P. H. 1972, J. Phys. Chem. Ref. Data, 1, 423
Liu, X.-W., Barlow, M. J., Danziger, I. J., and Clegg, R. E. S. 1995, MNRAS, 273, 47
Meinel, A. B. 1950a, ApJ, 111, 433
Meinel, A. B. 1950b, ApJ, 112, 464
Moore, C. E. 1945, Cont. Princeton Univ. Obs., 20, 1
Osterbrock, D. E., and Martel, A. 1992, PASP, 104, 76
Osterbrock, D. E., Walker, M. F., and Koski, A. T. 1976, PASP, 88, 349
Reynolds, R. J. 1990, in Galactic and Extragalactic Background Radiation, IAU Symposium No. 139, ed. S. Bowyer and C. Leinert (Dordrecht, Kluwer), p. 157
Vogt, S., et al. 1994, SPIE Conference 2198, 361

© Astronomical Society of the Pacific • Provided by the NASA Astrophysics Data System